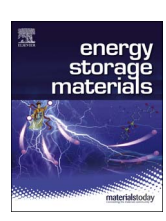
ELSEVIER

Contents lists available at ScienceDirect

Energy Storage Materials

journal homepage: www.elsevier.com/locate/ensm



Unveiled correlations between electron affinity and solvation in redox potential of quinone-based sodium-ion batteries



Ki Chul Kim^{a,b,*,1}, Tianyuan Liu^{c,1}, Ku Hyun Jung^b, Seung Woo Lee^{c,d,**}, Seung Soon Jang^{a,d,e,f,***}

- a Computational NanoBio Technology Laboratory, School of Materials Science and Engineering, Georgia Institute of Technology, Atlanta, GA 30332, USA
- ^b Department of Chemical Engineering, Konkuk University, Seoul 05029, Republic of Korea
- ^c G. W. Woodruff School of Mechanical Engineering, Georgia Institute of Technology, Atlanta, GA 30332, USA
- $^{
 m d}$ Institute for Electronics and Nanotechnology, Georgia Institute of Technology, Atlanta, GA 30332, USA
- ^e Parker H. Petit Institute for Bioengineering and Bioscience, Georgia Institute of Technology, Atlanta, GA 30332, USA
- f Strategic Energy Institute, Georgia Institute of Technology, Atlanta, GA, 30332, USA

ABSTRACT

First-principles density functional theory method is employed with experimental techniques to investigate the redox properties and charge storage performance of seven quinone derivatives and to assess their potential as cathodes in sodium-ion batteries. The computed redox properties are comprehensively correlated with other properties, namely, electron affinity (EA), solvation energy, charge storage capacity, and energy density. The correlations are further verified to be applied not only to quinones but also to other organic molecules. The established *universal* correlations highlight three main conclusions. First, EA and solvation energy need to be cooperatively tuned to achieve a specific redox potential. Second, the exceptionally high performance of anthraquinone-2,6-dicarboxylic acid can be explained by the correlation of the redox potential with EA and solvation energy. Third, the differences in the performance between the calculated and experimental values for the other six quinone derivatives mainly result from the Na binding configurations, highlighting the experimental charge capacity is extraordinarily enhanced by metastable Na binding scenarios.

1. Introduction

Sodium-ion batteries (SIBs) have recently attracted significant attention as the most promising technology for replacing lithium-ion batteries (LIBs) owing to the low cost driven by the abundance of sodium resources [1-8]. In the pursuit of high-performance electrode materials for SIBs, organic materials have attracted particular attention due to several advantages such as low cost with large-scale production, environmental friendliness, sustainability, and structural diversity [2,3,6,9,10]. In addition, the structural changes of organic materials during the redox reactions with metal ions are very small compared to inorganic materials [11,12].

Considerable efforts have been recently made to identify promising organic cathode materials with better performance such as high energy densities as well as enhanced redox potential. In the early stage, a variety of conducting polymers such as polypyrroles [2,3] and

polythiophenes [13] have been investigated as promising cathode materials in SIBs and their potential has been evaluated. For example, Wang and coworkers reported that hollow polypyrrole nanospheres exhibited superior rate capability and sustained cycling stability [2]. Yang and coworkers proposed an aniline/o-nitroaniline copolymer with the high potential and strong capacity retention as cathode materials in SIBs [13]. They reported that PF₆⁻ anions in the electrolyte would be doped into and de-doped from the polymer during the charging and discharging processes, respectively [13]. Very recently, the efforts have been extended from anion-driven p-type polymers into cation-driven n-type organic molecules, aiming at the identification of promising cathode candidates with higher energy densities for rechargeable batteries [14-28]. Carbonyl-based compounds, which can reversibly bind with Li- or Na-ions via carbonyl groups, has attracted intensive interests [14-22]. The past few years have witnessed the efforts in understanding their redox properties through

^{*} Corresponding author at: Department of Chemical Engineering, Konkuk University, Seoul 05029, Republic of Korea.

^{**} Corresponding author at: G.W. Woodruff School of Mechanical Engineering, Georgia Institute of Technology, Atlanta, GA 30332, USA.

^{***} Corresponding author at: Computational NanoBio Technology Laboratory, School of Materials Science and Engineering, Georgia Institute of Technology, Atlanta, GA 30332, USA E-mail addresses: kich2018@konkuk.ac.kr (K.C. Kim), seung.lee@me.gatech.edu (S.W. Lee), seungsoon.jang@mse.gatech.edu (S.S. Jang).

 $^{^{\}mathbf{1}}$ These authors contributed equally to this work.

either experimental or computational methods [23–28]. For instance, Dunn and coworkers synthesized naphthalene diimide derivatives with tailored functionalities, and showed that redox potentials varied from 2.3 to 2.9 vs. Li/Li⁺ with different substituted functional groups [23]. In addition, Zhang and coworkers developed high-performance organic cathodes with enhanced redox potential and cyclic stability for SIBs through tailoring conjugated backbones in polyimides [29].

In addition, a few computational studies have been devoted to investigating the redox properties of quinone-based organic molecules for rechargeable secondary batteries [15,18,24,25]. Aspuru-Guzik and coworkers employed a large-scale computational screening approach to efficiently predict the redox potentials of a broad array of quinone derivatives for redox flow battery applications [24]. Assary and coworkers investigated the redox potentials associated with the transfers of the first and second electron(s) into anthraquinone derivatives [25]. In our previous studies, we investigated the redox potentials of various quinone-based organic molecules as cathode materials in LIBs [15,18]. Despite all these significant efforts, the progress in understanding the redox properties of the organic molecules is still limited to tuning their redox potentials by employing structural variations on their design. Fundamental understanding of their redox properties in a correlation with other parameters, such as electron affinity (EA) and solvation, is not thoroughly accomplished yet. In particular, there is no study on the redox properties of organic molecules interacting with sodium atoms during the discharging process, which is essential for the improvement of the cell performance. Thus, a guideline for the rational design of novel organic cathode materials is highly desired.

In this study, we aimed at achieving fundamental understanding of the redox properties of quinone-based organic molecules by seeking their correlation with key parameters, such as EA and solvation energy, and evaluating their potential in terms of their performance for SIB applications. For this goal, we investigated the seven quinone derivatives (see Fig. 1), namely 1,4-benzoquinone (BQ), 1,4-naphthoquinone, 9, 10-anthraquinone (AQ), 2-aminoanthraquinone (AAQ), 2,6-diaminoanthraquinone (DAQ), anthraquinone-2-carboxylic acid (CAQ), and anthraquinone-2,6-dicarboxylic acid (DCAQ), which were employed in our previous study [18]. The contribution of the EA and solvation energy to the redox potential are systematically scrutinized for the organic molecules bound with Na atoms during the discharging process. This analysis is further extended to their theoretical charge and energy capacities, aiming at the design of the complete correlation of the EA – solvation energy – redox potential – theoretical performance.

2. Materials and methods

2.1. Computational section

2.1.1. Na binding energies and binding free energies

All of the calculations were performed by using Jaguar with 6–31 G+(d,p) basis set and PBE0 level of theory [30]. The Na binding energies (ΔE_b) of the seven quinone derivatives, namely 1,4-benzoquinone, 1,4-naphthoquinone, 9,10-anthraquinone, 2-aminoanthraquinone, 2,6-diaminoanthraquinone, anthraquinone-2-carboxylic acid, and anthraquinone-2,6-dicarboxylic acid, in vacuum can be predicted by Eq. (1) as,

$$\Delta E_b = E_{0, (O+Na)} - E_{0,O} - E_{0,Na} \tag{1}$$

Here, $E_{0,Q}$, $E_{0,Na}$, and $E_{0,(Q+Na)}$ represent the density functional theory (DFT) calculated total energies for the geometrically optimized models of a bare quinone derivative, Na atom, and quinone derivative with Na, respectively. For each system containing a quinone derivative with Na, all conceivable Na binding sites were considered to systematically and reliably identify a most stable configuration of the system.

To predict the Na binding free energies (ΔG_b) of the seven quinone derivatives in vacuum, the vibrational and entropic contributions to the free energies were considered by Eq. (2) as,

$$\Delta G_b = G_{Q+Na} - G_Q - G_{Na} \tag{2}$$

Here, G_Q , G_{Na} , and G_{Q+Na} represent the Gibbs free energies for the geometrically optimized models of the bare quinone derivative, Na atom, and quinone derivative with Na, respectively. The Gibbs free energy can be defined by Eq. (3) as,

$$G = (E_0 + E_{vib} + PV) - TS \tag{3}$$

Here, E_{vib} , P, V, T, and S represent the vibrational energy, pressure, volume, temperature, and entropy, respectively. The computed Na binding free energies of the seven quinone derivatives in vacuum can be finally converted into those (ΔG^{soln}) in solution by incorporating the solvation free energy for each of the bare quinone derivative, Na atom, and quinone derivative with Na into the Eq. (2).

2.1.2. Redox potentials

All of the calculations were performed by using the Jaguar with a 6–31 G+(d,p) basis set. Both the PBE0 and PWB6K levels of theory were chosen to compute the optimized geometries of the seven quinone

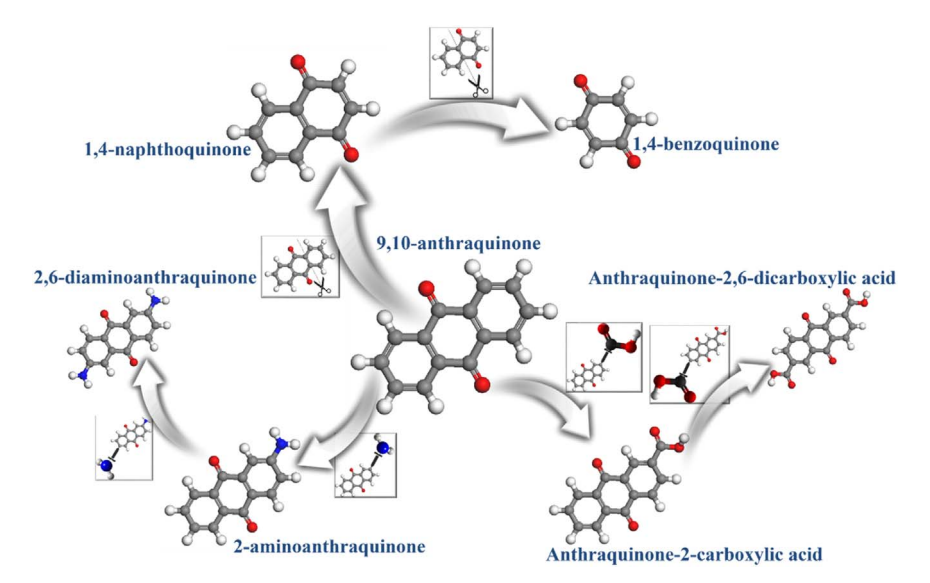


Fig. 1. Chemical structures of the seven quinone derivatives. Structures of 1,4-benzoquinone (BQ), 1,4-naphthoquinone (NQ), 9,10-anthraquinone (AQ), 2-aminoanthraquinone (AAQ), 2,6-diaminoanthraquinone (DAQ), anthraquinone-2-carboxylic acid (CAQ), and anthraquinone-2,6-dicarboxylic acid (DCAQ). The atoms in gray, white, red, and blue correspond to carbon, hydrogen, oxygen, and nitrogen, respectively.

derivatives either with or without Na binding [30]. The vibrational frequency calculations, with the same levels of theory and basis set, were further computed to evaluate the Gibbs free energies at 298 K in vacuum. The solvation free energy calculations were computed using Poisson-Boltzmann implicit solvation model to approximate the solvation contributions to the free energies [31]. A dielectric constant of 16.14, which reliably describes the polarity of the solvents of ethylene carbonate (EC) and dimethyl carbonate (DMC) in mixture (3:7 v/v) in our systems, was used for the solvation free energy calculations.

The thermodynamic cycle which was used to predict the redox potentials of the quinone derivatives is described elsewhere [15–19,32]. The redox potential (ΔE^{red}) of an active positive electrode material in solution with respect to a Na/Na⁺ reference electrode can be predicted by Eq. (4) as,

$$\Delta E^{red} = \frac{-\Delta G^{soln}}{nF} - 1.73V \tag{4}$$

where, ΔG^{soln} is the difference in the Gibbs free energy in solution during the reduction, n is the number of electrons transferred, and F is the Faraday constant [32,33]. The constant, 1.73 V, indicates the redox potential of the Na/Na⁺ reference electrode. The electronic properties (the HOMO and LUMO energy levels as well as the electron affinity) of the active positive electrode materials were also computed to rationalize the predicted redox potentials.

2.1.3. Correlation of electron affinity – solvation energy – redox potential

According to the thermodynamic cycle, the difference in the Gibbs free energy of a quinone in solution phase during the reduction is defined by the sum of the EA and solvation energy [15–19,32]. Here, the EA (ΔG^{gas}) is the change in the Gibbs free energy of the quinone during the reduction in gas phase. The solvation energy ($\Delta \Delta G^{solv}$) is the change in the solvation free energy of the quinone through its state change from the neutral state to the anionic state in the solvent phase as defined by $\Delta \Delta G^{solv} = \Delta G^{solv}(R^-) - \Delta G^{solv}(R)$, where $\Delta G^{solv}(R^-)$ and $\Delta G^{solv}(R)$ denote the solvation free energies of the anionic and neutral states, respectively. Thus, the difference in the Gibbs free energy of a quinone in solution phase during the reduction is described as $\Delta G^{soln} = \Delta G^{gas} + \Delta \Delta G^{solv}$. Combined with the reorganized form of Eq. (4), namely $\Delta G^{soln} = -nF(\Delta E^{red} + 1.73)$, the final equation is defined by $\Delta \Delta G^{solv} = -nF(\Delta E^{red} + 1.73) - \Delta G^{gas}$.

2.1.4. Theoretical charge capacities and energy densities

The theoretical charge densities (Q) of the seven quinone derivatives, describing the maximum number of Na atoms that would be stored in the molecules, were computed by

$$Q(Ah/kg) = \frac{nF}{3.6M_w} \tag{5}$$

Here, M_{ν} denotes the molecular weight in mol/g. For the calculations, each Na atom was assumed to be placed in the thermodynamically most stable position. The predicted charge densities of the molecules were then employed to reliably compute their energy densities (W) which would be defined by [11]

$$W(Wh/kg) = \int_0^Q V(q)dq \tag{6}$$

2.2. Experimental section

All the organic molecules were purchased from Sigma-Aldrich, *p*-Benzoquinone (BQ), 1,4-Naphthoquinone (NQ), Anthraquinone (AQ), Anthraquinone-2-carboxylic acid (CAQ), 2-Aminoanthraquinone (AAQ), 2,6-Diaminoanthraquinone (DAQ). The few-walled carbon nanotubes (FWNTs) were synthesized by chemical vapor deposition method according to previous papers [34,35]. A mixture of FWNTs (3

mg) and organic molecules (3 mg) was added to DI- $\rm H_2O$ (15 ml). The solutions were sonicated for overnight. The solution was filtered through a Celgard 3501 membrane, then the obtained composite films were dried at 70 °C for overnight.

The electrochemical measurement was conducted using two electrode Swagelok cells. A piece of Na foil was used as anode, the composite films were directly used as cathodes, and two pieces of Celgard 2500 were used as separators. The electrolyte used was 1 M NaPF $_6$ in ethylene carbonate (EC) and dimethyl carbonate (DMC) (3:7 v/v, BASF). All the cells were assembled in an argon filled glovebox (MBraun). The electrochemical measurements were conducted using Bio-Logic VMP3 potentiostat/galvanostat at room temperature. The reduction potentials were measured using cyclic voltammetry in the voltage window of 1.0–4.0 V vs. Na.

3. Results and discussion

The seven quinone derivatives with different backbone lengths and functionalities were adapted from our previous study [18]. Fig. S1 in Supplementary information shows the DFT-calculated redox potentials of the pristine quinone derivatives, which were compared with values experimentally measured from cyclic voltammetry (Fig. S2 in Supplementary information). Our DFT-computed results showed an uncertainty of $\sim 0.3 \, \text{V}$ as compared with the electrochemical measurements, indicating the reliability of our computational protocol. The highly accurate computational protocol allowed us to draw solid conclusions by systematically analyzing the redox properties and performance of the quinone derivatives in the following sections.

Note that another computational approach utilizing the Na-binding reaction scheme has been also reported to calculate the redox potentials of materials [36–38]. However, this approach usually requires the well-defined positions of Na atoms in the materials to predict the redox potentials, which is not trivial usually due to the uncertainty in predicting accurate crystalline structure. In addition, the molecular electrochemical reduction process occurs before the molecules accommodate sodium cations during the discharging process. Therefore, our approach estimating the intrinsic electrochemical reduction potential of molecules, would be very useful for the organic materials whose sodiated structures are not known clearly.

Further, please note that the quinone derivatives can be chemically bound onto conductive carbon materials, such as graphenes and carbon nanotubes, which would be a strategy to use the quinone derivatives in cathodes by preventing the molecular dissolution [39]. Polymerization is another strategy to resolve this issue [39]. Liu et al. demonstrated the high cycling stability with self-polymerized dopamines which were spontaneously coated on the surfaces of few-walled carbon nanotubes, indicating the successful incorporation of organic molecules in cathodes [16].

3.1. Redox properties of quinones at thermodynamic equilibrium state

The redox properties of organic molecules employed for the cathodes in SIBs are generally considered to depend on their electronic structures. Our previous study has also shown that the interactions between organic molecules and Li during the charging and discharging processes will affect their redox properties [18]. Thus, to obtain a comprehensive understanding of their redox properties in SIBs, we first determined the most energetically favorable binding sites for Na atoms at each sodiation step by considering a vast number of possible positions for Na binding. Only configurations with most energetically favorable Na binding were further investigated for predicting their redox potentials. Meanwhile, the electronic structures of sodiated molecules were also discussed.

Fig. 2 shows the general aspect on the effects of aromaticity, functionality, and Na binding thermodynamics on the redox properties

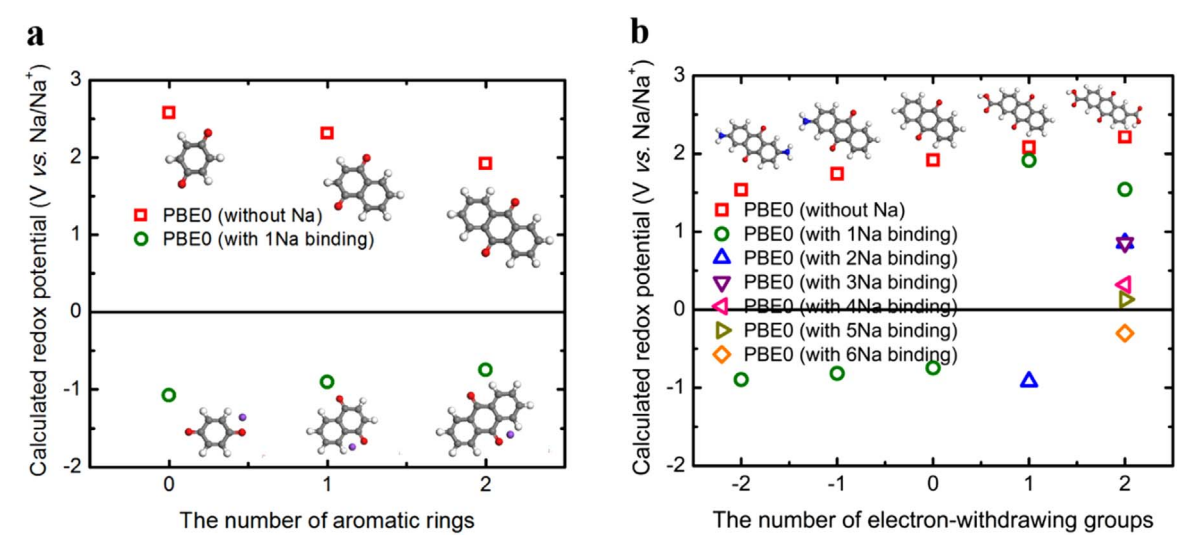


Fig. 2. Redox potential correlations (as determined using the PBE0 functional). Correlations of the redox potential with (a) backbone aromaticity and (b) functionalities based on the most stable Na binding configurations. In a, the number of aromatic rings in BQ, NQ, and AQ are zero, one, and two, respectively. In b, the redox potentials are depicted as a function of the number of electron-donating (i.e., -NH₂) or electron-withdrawing (i.e., -COOH) groups incorporated in AQ. On the x-axis, the numbers of electron-donating and electron-withdrawing groups are denoted by negative and positive integers, respectively. The PWB6K-based results are shown in the Supplementary information.

of the quinone molecules at equilibrium. Three main features were highlighted from these comparisons.

First, the redox potentials of the bare molecules could be tuned in the desired direction by systematically modifying their structures or functionalities. Increasing the number of aromatic rings from zero (BQ) through one and to two (AQ) aromatic rings (Fig. 2a) decreases the redox potential of quinone derivatives as shown by the red square symbol. On the other hand, the redox potential could also be tuned by incorporating functional groups, increasing (decreasing) the redox potential with incorporating electron withdrawing carboxylic acids (donating amines).

Note that these trends in SIBs are similar to those in LIBs, suggesting that general nature of redox properties would be independent of the battery type [18], which can be explained by chemical intuition: the electron-withdrawing or electron-donating functional groups would make the main redox-active carbonyls either more electrophilic or nucleophilic, respectively. Similar conclusions were also confirmed in other studies. Aspuru-Guzik and coworkers predicted in their database that BQ had the highest redox potential among all the quinone derivatives [24]. They also showed that incorporating electron-withdrawing functional groups could increase the redox potential. Likewise, Assary and coworkers showed that increasing the number of electron-withdrawing chloro groups in AQ could further increase its redox potential [25].

Second, the redox potential of sodiated-quinone derivatives was continuously decreased as Na atoms were progressively added into the molecule during the discharging process. The insertion of Na atom into the molecule could weaken the electrophilicity of the molecule. Third, most importantly, our calculations predict that the number of Na atoms stored in a quinone at their most stable positions through sodiation during the discharging process would generally depend on the number of carbonyl groups in the molecule. Note that a quinone anion reduced by the addition of an electron attracts a Na cation to form a quinone-Na complex, which is repeated during the discharging process. Thus, the complex needs to sustain its reductive ability (i.e., positive redox potential) to accept additional Na atoms as cathode. The electrondeficient nature of the quinone backbone is strengthened with the increase in the number of electron-withdrawing carbonyls due to the inductive effect. This leads to the increase of the number of Na atoms stored in the molecule with sustaining its reductive ability. Specifically, in Fig. 2, it is shown that five quinone derivatives (BQ, NQ, AQ, AAQ, and DAQ) with one bound Na atom near carbonyl moieties have negative redox potentials with respect to Na metal anode, meaning that they lose their cathodic activities after they accept one Na. This indicates that each of them could store only one Na atom.

In contrast, CAQ with a carboxylic functional group (*i.e.*, carbonyl moiety) showed a negative redox potential after binding with two Na atoms, suggesting a theoretical charge capacity is two Na atoms per molecule. Surprisingly, DCAQ which was generated by the addition of another carboxylic functional group into CAQ, resulted in a significant increase in the number of stored Na atoms, sustaining its cathodic activity (*i.e.*, a positive redox potential) even after binding with five Na atoms. This indicates that six Na atoms can be theoretically stored into each DCAQ.

For all the seven quinone derivatives, the first Na atom was preferentially bound near one of the two main redox-active carbonyls as illustrated in Fig. S4 in the Supplementary information. It is worthwhile to note that a certain amount of electronic charge (0.7 - 0.8e) was transferred from Na atom to each quinone, and the degree of the charge transfer was further increased by 0.11 - 0.12e in dielectrically polarized environment (Fig. S5 in the Supplementary information). Note that organic solvents of ethylene carbonate and dimethyl carbonate in electrolytes generate the dielectric polarization [40]. In CAQ and DCAQ, the second Na atom preferred to bind to the other carbonyl group. Once the two main redox-active carbonyls in the DCAQ were occupied by two Na atoms, two more Na atoms could be favorably positioned to the carbonyl moieties in the carboxylic groups. Lastly, two more Na atoms could be further added next to the first two bound Na atoms, resulting in two Na atoms binding to each central carbonyl. This is unusual in comparison to our previous studies on quinones [18] and dopamines [16] where only one Li atom could be bound to each carbonyl. This leads to the unexpectedly high Na charge capacity of DCAQ.

3.2. Computed performance vs. experimental performance

The afore-mentioned understanding on the change in the redox potentials of the quinones during the discharging process allows us to estimate their theoretical charge capacities and energy densities as shown in Figs. S6 and S7 in the Supplementary information. These two theoretical performance parameters were computed using Eqs. (5) and (6) by assuming the maximum number of Na atoms stored into each quinone at thermodynamic equilibrium state. Here, Na atoms were assumed to occupy the most stable positions from the thermodynamic point of view at each sodiation stage. We highlight a remarkable

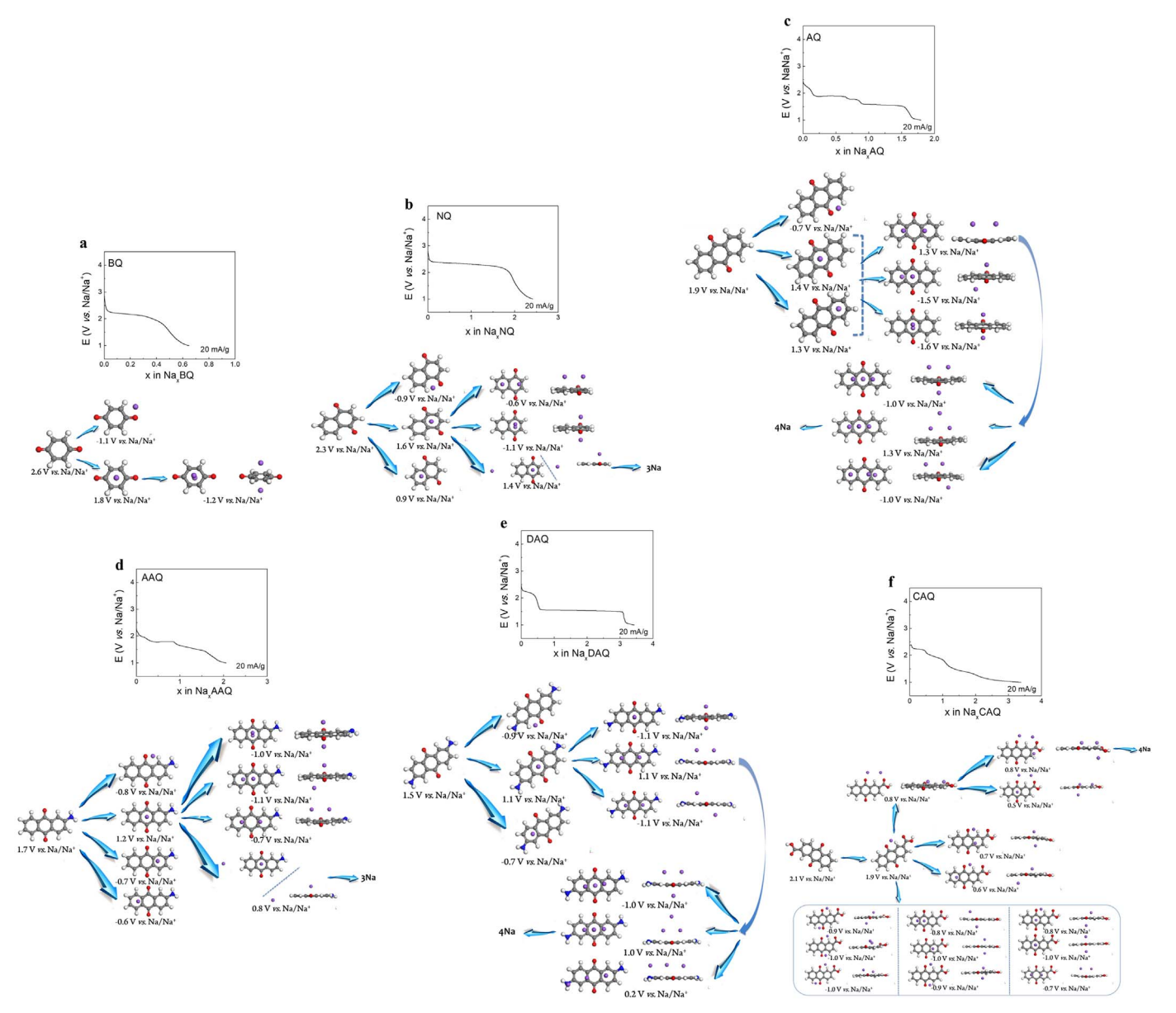
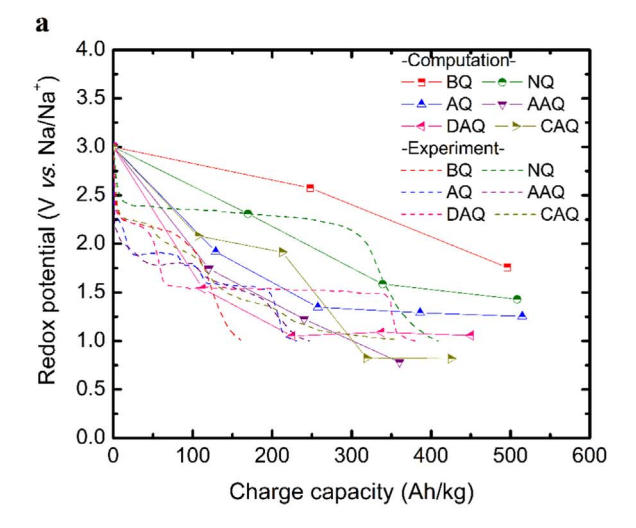


Fig. 3. Possible Na binding scenarios (as determined using the PBE0 functional) for the six experimentally available quinone derivatives. Bindings of (a)BQ, (b)NQ, (c)AQ, (d)AAQ, (e)DAQ, and (f)CAQ, with Na atoms at their metastable positions. The number of Na atoms corresponds to the experimental charge capacity for each quinone derivative, which is shown as a function of the cell voltage.

observation in which the DCAQ was predicted to exhibit higher theoretical charge capacity (543 Ah/kg) and energy density (536 Wh/kg) in comparison to any other cathode materials reported for LIBs and SIBs [1,41,42]. The theoretical performance parameters would be constant because Na atoms would be strongly bound to the DCAQ. Note that both of the redox potential and charge capacity would contribute to the energy density based on the definition of the energy density in Eq. (6). Thus, the capability of the DCAQ storing a large number of Na atoms during the discharging process would lead to such a high energy density. In contrast, our electrochemical measurements for experimentally available six quinones revealed that five of the quinones, namely the NO, AO, AAO, DAO, and CAO, showed much higher specific capacities than our theoretical results. Such an unexpected disagreement was not observed in our previous study for LIBs, indicating that Na atoms might not be placed in their most stable positions owing to kinetic limitation such as the blockage of main redox-active carbonyls [18].

To explain this unexpected discrepancy between our computational and experimental results, we explored various discharge scenarios associated with metastable Na binding for each quinone as shown in

Fig. 3. Specifically, under the assumption that the most stable Na binding configurations would not be available owing to a steric hindrance or kinetic limitation, we focused on identifying other Na binding configurations that could meet the experimental charge capacity sustaining the redox potential higher than 0.7 V vs. Na/Na⁺ (considering the afore-mentioned DFT uncertainty of 0.3 V vs. Na/ Na⁺) for each quinone. For instance, the experimental charge capacity (1.8 Na atoms per AQ in average) of AQ can be rationalized by the storage of at least four Na atoms in a discharge scenario associated with metastable Na binding, as shown in Fig. 3c. The resultant profiles for the charge capacity and energy density that reflect the explored Na binding scenarios are shown in Fig. 4, exhibiting a great agreement between experiment and computation. A striking observation from the figures was that such extraordinarily high charge capacities would be feasible if extra Na atoms were able to bind weakly with quinone-Na complexes. For instance, in the case of the DAQ with two Na atoms symmetrically bound on top of aromatic rings, the third Na atom was predicted to be weakly bound on top of the two bound Na atoms sustaining the redox potential of 1.0 V vs. Na/Na⁺. Thus, it is reason-



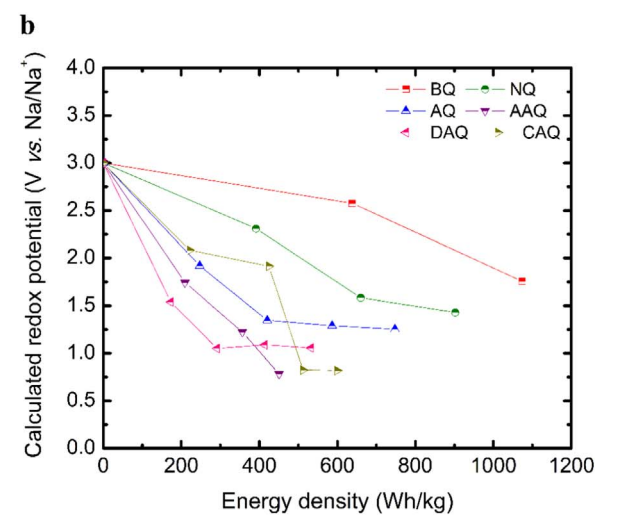


Fig. 4. Profiles of the calculated redox potential (as determined using the PBEO functional). Calculated redox potential vs. (a) charge capacity and (b) energy density for the six experimentally available quinone derivatives binding with Na atoms at metastable positions according to the scenarios described in Fig. 3 during the discharging process. The experimentally measured charge capacities are also shown.

ably expected from the observation that the experimental charge capacities might be fluctuated with the possible release of weakly bound Na atoms. Note that the nature of the smallest quinone, BQ, being easily dissolved by organic solvents might have led the quinone to have a relatively low experimental charge capacity despite the expectation of the analogous situation with the five quinones stated above.

3.3. Correlation of electron affinity – solvation energy – redox property

Our previous studies on the Li-based redox properties of quinones and carbon materials have shown two main features [15–19]. (i) Organic molecules would sustain the cathodic activity exhibiting positive redox potentials until each carbonyl could bind with one Li and thereby no carbonyl is available for further Li binding. (ii) The cathodic activity would strongly rely on the solvation energy. Organic molecules with negative solvation energy (i.e., solvation free energy at the neutral state > solvation free energy at the anion state) would be cathodically active exhibiting positive redox potentials. However, the results predicted on the basis of the most stable Na binding configurations in this study do not follow the first feature as stated in the

previous section. In addition, the solvation energy – redox property correlation suggested in the second feature is not mature enough to be utilized to establish a design strategy for promising cathode materials in SIBs. For instance, DCAQ with six Na atoms bound at their most stable positions became cathodically inactive, exhibiting a negative redox potential despite its negative solvation energy (see Fig. 5a). Thus, the correlations of three key components, namely EA, solvation energy, and redox property, were comprehensively investigated in three approaches to unveil fundamental structure-property relationships.

The simplest way to explain the redox properties of the seven quinone derivatives was to correlate the redox properties with their electronic structures, such as the EA, lowest unoccupied molecular orbital (LUMO), and highest occupied molecular orbital (HOMO) for both the most stable and metastable Na binding cases, as shown in Fig. S9 in the Supplementary information. It seems that the linear correlations of the redox potential with the EA, LUMO, HOMO, and HOMO-LUMO gap were observed within the range of positive redox potentials. It was particularly highlighted that the more negative values for EA, LUMO, and HOMO would have higher redox potentials for quinones with more reductive ability while the more positive value of HOMO-LUMO gap would be related to higher redox potential. Similar observations had been consistently reported from other studies and our previous studies [15-19,43]. It was, therefore, concluded that the EA and LUMO would be indicators to predict the redox potentials of various organic molecules unless the redox potentials are negative.

To provide a better understanding on the redox properties of quinones, we correlated their redox potentials with either of two primary contributors to determine the redox properties, namely EA and solvation energy as shown in Fig. 5 for the most stable Na binding configurations and Fig. S10 in the Supplementary information for the metastable Na binding configurations. This approach could draw the main conclusion: the cathodic activity would strongly rely on the solvation energy and thereby a positive solvation energy would generally lead to a negative redox potential. Our previous study had also correlated the redox properties with these two contributors independently [18]. Here, the contributions of EA and solvation energy are defined by the changes in its Gibbs free energy and solvation free energy during its state changes from the neutral to anionic state, respectively. Note that a negative value for the EA (solvation energy) means that the anionic state is thermodynamically more stable (preferred to be solvated) as compared with the neutral state. The EA was always negative regardless of the quinone type and number of the bound Na atoms, indicating that the reduced state would be always more preferred than the neutral state. In contrast, the solvation energy relied on the Na binding state significantly. For the most stable Na binding configurations, five quinone derivatives, namely the BQ, NQ, AQ, AAQ, and DAQ, exhibited negative values for the solvation energy of these pristine molecules, while the solvation energy turned into positive after one Na bound to these quinones. The changes in the solvation energy from negative to positive values suggest that the anionic state would become less favorable to be solvated than the neutral state, resulting in negative redox potentials. Likewise, CAQ binding with 2 Na atoms exhibited a positive value for the solvation energy, leading to a negative redox potential. However, to be noted, DCAQ with six bound Na atoms did not follow this correlation, exhibiting a negative redox potential despite its negative value for the solvation energy. This indicates that this approach is not still sufficient to perfectly describe the structure-property relationships. Note that, for the metastable Na binding cases, all exhibited negative values for the solvation energy, leading to positive redox potentials.

Thus, a comprehensive and robust correlation that can be applied to any organic molecules for cathodes in SIBs without exception is necessarily built as the last approach. The novel correlation established in the final stage using Eq. (4) is defined by

$$z = -nF(x+1.73) - y = -23.061(x+1.73) - y$$
(7)

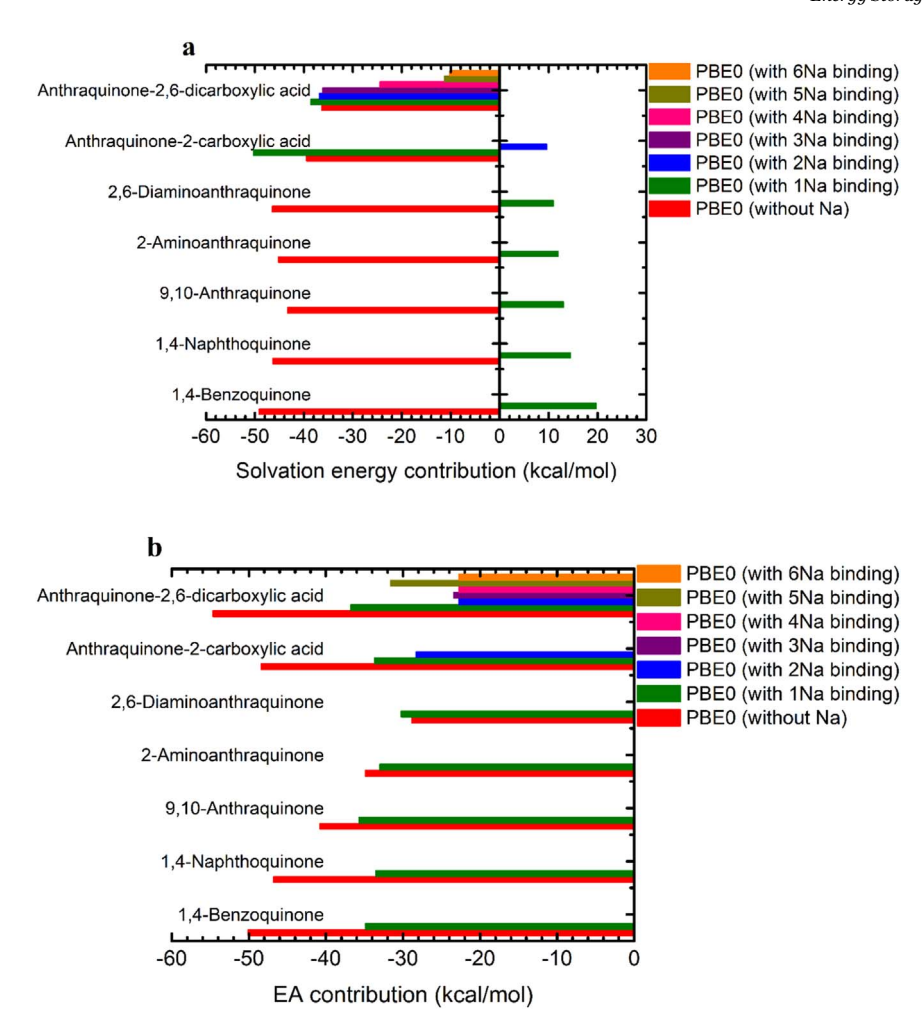
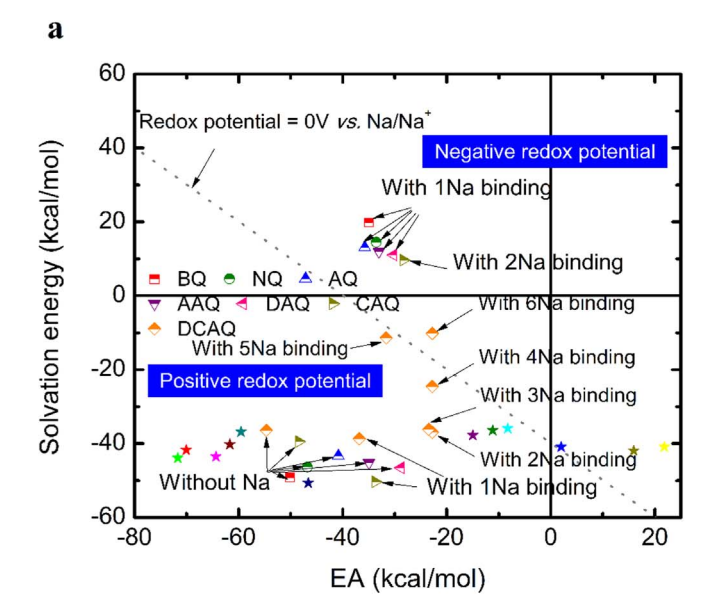


Fig. 5. Contributions to the redox potentials of the seven quinone derivatives. Contributions of (a) the solvation energy and (b) electron affinity (EA) to the redox potential (as determined using the PBE0 functional) based on the most stable Na binding configuration. The PWB6K-based results are shown in the Supplementary information.

Here, x, y, z, n, and F denote the redox potential in V vs. Na/Na⁺, EA in kcal/mol, solvation energy in kcal/mol, number of electrons transferred, and Faraday constant, respectively. Note that this equation can be simplified into y + z = -40 at the zero-potential. It needs to be highlighted that this approach describes the correlations between the EA and solvation energy not only to determine the sign of the redox potential but also to predict a specific value of the redox potential for each molecule with/without Na atom(s) bound at the most stable position(s). (see Figs. 6a and 6b) The same figures containing a set of molecules with/without Na atom(s) bound at metastable position(s) are shown in Fig. S12 in the Supplementary information. As shown in Fig. 6a, the rule of 'a positive redox potential at a negative solvation energy' stated earlier will not be always true if the EA is greater than -40 kcal/mol. Thus, the case of the DCAQ with six bound Na atoms having the EA of -23 kcal/mol would exhibit the negative redox potential of -0.3 V vs. Na/Na⁺ despite the solvation energy of -10 kcal/mol. Fig. 6b provides a comprehensive understanding on the correlation between the EA and solvation energy that should be satisfied to sustain a given positive redox potential. For instance, a quinone having the EA of -40 kcal/mol would have to sustain a solvation energy within the range of $-25 \sim 0$ kcal/mol to show a redox potential of 1 V vs. Na/Na⁺. Likewise, a quinone having the EA of -90 kcal/mol would have to sustain a solvation energy lower than 50 kcal/mol to show a positive redox potential. It can be concluded that the highest value for the solvation energy required to sustain a positive redox potential would increase with decreasing the EA. It is further emphasized that these correlations are applied not only to quinones but also to other organic molecules as shown in Fig. 6 for various organic molecules, such as

trichloro isocyanuric acid, trifluoro isocyanuric acid, caffeine, ascorbic acid, dehydroascorbic acid, pramipexole, dihydroxyindole, indolequinone, corannulenes, and coronenes, indicating that the suggested correlation can be generalized. The structures of the organic molecules are shown in Fig. S13 in the Supplementary information.

Finally, it is highlighted from Fig. 6 that the DCAQ and CAQ would experience a two-stage non-simultaneous transition of the EA and solvation energy during the Na binding unlike the others. The DCAQ would experience the continuous transition of the EA toward a less negative value without a significant change in the solvation energy up to the binding of two Na atoms followed by the continuous transition of the solvation energy toward a less negative value without a significant change in the EA during the binding of three to six Na atoms. Regarding the EA behavior in vacuum, as shown in Fig. S14 in the Supplementary information, the HOMO and LUMO of the DCAQ-Na complex would increase with the bound Na atoms up to two Na binding (to the central carbonyls), indicating the Na binding weakens the EA. Once two Na atoms are bound to the DCAQ, the HOMO and LUMO of the complex would be converged, resulting in the negligible effect of the additional Na binding (to the carboxylate carbonyls and Na-bound central carbonyls) on its energy diagram and reduction ability. This suggests that the first two Na atoms bound to the central carbonyls would significantly change the electronic structure of the DCAQ as compared with the subsequent, weak Na binding to the carboxylate carbonyls and central carbonyls. This also indicates that the first two Na binding to make DCAQ-1Na and DCAQ-2Na will entail unique electronic structures in solution phase, which are stabilized well without sacrificing the solvation energy. In contrast, further addition of Na would generate a



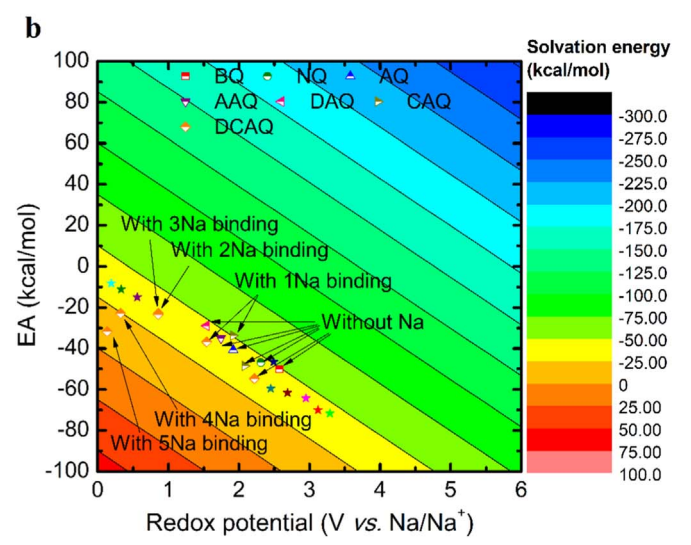


Fig. 6. Correlations between the EA and the solvation energy. Correlations to (a) determine the sign of the redox potential and (b) predict a specific redox potential within the range of 0−6 V vs. Na/Na⁺. The data points (as determined using the PBE0 functional) correspond to the seven quinone derivatives with or without bound Na atom(s) at the most stable position(s). The PWB6K-based results are shown in the Supplementary information. Data points for twelve different organic molecules, namely trichloro isocyanuric acid (3.12 V vs. Na/Na⁺, →), trifluoro isocyanuric acid (3.29 V vs. Na/Na⁺, →), ascorbic acid (0.19 V vs. Na/Na⁺, →), dehydroascorbic acid (2.95 V vs. Na/Na⁺, →), pramipexole (−0.90 V vs. Na/Na⁺, →), 5,6-dihydroxyindole (−0.60 V vs. Na/Na⁺, →), 5,6-indolequinone (2.49 V vs. Na/Na⁺, →), coronnel (0.33 V vs. Na/Na⁺, →), 1B-doped coronnulene (2.69 V vs. Na/Na⁺, →), are also provided to verify the generalization of the correlations. The structures of the organic molecules are shown in Supplementary information.

weak binding without a significant hybridization in their electronic structures. Thus, the introduction of an electron to the complexes in solution phase would lead to the incomplete-stabilization, sacrificing he solvation energy toward a less negative value.

4. Conclusion

In this study, we investigated the fundamental relationships between the redox properties and performance parameters of seven quinone derivatives with various Na binding states during the discharging process for SIB cathodes. Correlation of the DFT-calculated redox properties with the EA and solvation energy highlighted that the cathodic activity of a quinone with a positive redox potential could be sustained by systematically tuning both the EA and solvation energy. The highest solvation energy required to sustain a positive redox potential would increase with decreasing EA. The correlations were further verified to be applied not only to quinones but also to other organic molecules. The established *universal* correlations will allow us to systematically design promising organic molecules (which would not be limited to quinones) with desired redox properties and performance for SIB cathodes.

Extension of our efforts to reliably correlate the redox properties and electronic structures of quinones to the prediction of charge storage performance based on the maximum number of bound Na atoms revealed the following striking features. (1) The exceptionally high charge capacity and energy density computed for DCAQ can be explained by correlation of the redox potential with the EA and solvation energy. (2) The computational performance parameters were much lower than the experimental observation for NQ, AQ, AAQ, DAQ, and CAQ. This deviation was verified to result from extraordinary enhancement of the experimental charge capacity by metastable Na binding configurations.

Acknowledgments

General: All authors have given approval to the final version of the manuscript.

Funding

This work was supported by the National Research Foundation of Korea (NRF) funded by the Ministry of Science, ICT & Future Planning (NRF-2017R1C1B5017482). This work was supported in part by the National Science Foundation under Grant no. 1805052.

Author contributions

The manuscript was written through contributions of all authors.

Competing interests

There are no conflicts of interest to declare.

Appendix A. Supplementary material

Supplementary data associated with this article can be found in the online version at doi:10.1016/j.ensm.2019.01.017.

References

- M.S. Islam, C.A.J. Fisher, Lithium and sodium battery cathode materials: computational insights into voltage, diffusion and nanostructural properties, Chem. Soc. Rev. 43 (2014) 185–204.
- [2] D. Su, J. Zhang, S. Doub, G. Wang, Polypyrrole hollow nanospheres: stable cathode materials for sodium-ion batteries, Chem. Commun. 51 (2015) 16092–16095.
- [3] L. Zhu, Y. Shen, M. Sun, J. Qian, Y. Cao, X. Ai, H. Yang, Self-doped polypyrrole with ionizable sodium sulfonate as a renewable cathode material for sodium ion batteries, Chem. Commun. 49 (2013) 11370–11372.
- [4] V. Palomares, P. Serras, I. Villaluenga, K.B. Hueso, J. Carretero-González, T. Rojo, Na-ion batteries, recent advances and present challenges to become low cost energy storage systems, Energy Environ. Sci. 5 (2012) 5884–5901.
- [5] J. Sun, H.-W. Lee, M. Pasta, H. Yuan, G. Zheng, Y. Sun, Y. Li, Y. Cui, A phosphorene–graphene hybrid material as a high-capacity anode for sodium-ion batteries, Nat. Nanotechnol. 10 (2015) 980–985.
- [6] L. David, R. Bhandavat, G. Singh, Mos2/graphene composite paper for sodium-ion battery electrodes, ACS Nano 8 (2014) 1759–1770.
- [7] S.-W. Kim, D.-H. Seo, X. Ma, G. Ceder, K. Kang, Electrode materials for rechargeable sodium-ion batteries: potential alternatives to current lithium-ion batteries, Adv. Energy Mater. 2 (2012) 710–721.
- [8] Y. Park, D.-S. Shin, S.H. Woo, N.S. Choi, K.H. Shin, S.M. Oh, K.T. Lee, S.Y. Hong, Sodium terephthalate as an organic anode material for sodium ion batteries, Adv. Mater. 24 (2012) 3562–3567.

- [9] S.W. Lee, B.M. Gallant, H.R. Byon, P.T. Hammond, Y. Shao-Horn, Nanostructured carbon-based electrodes: bridging the gap between thin-film lithium-ion batteries and electrochemical capacitors, Energy Environ. Sci. 4 (2011) 1972–1985.
- [10] M. Yao, H. Senoh, S.-i Yamazaki, Z. Siroma, T. Sakai, K. Yasuda, High-capacity organic positive-electrode material based on a benzoquinone derivative for use in rechargeable lithium batteries, J. Power Sources 195 (2010) 8336–8340.
- [11] J.B. Goodenough, K.-S. Park, The li-ion rechargeable battery: a perspective, J. Am. Chem. Soc. 135 (2013) 1167–1176.
- [12] L.P. Wang, L. Yu, X. Wang, M. Srinivasan, Z.J. Xu, Recent developments in electrode materials for sodium-ion batteries, J. Mater. Chem. A 3 (2015) 9353–9378.
- [13] R. Zhao, L. Zhu, Y. Cao, X. Ai, H.X. Yang, An aniline-nitroaniline copolymer as a high capacity cathode for na-ion batteries, Electrochem. Commun. 21 (2012) 36–38
- [14] Y. Wu, R. Zeng, J. Nan, D. Shu, Y. Qiu, S.-L. Chou, Quinone electrode materials for rechargeable lithium/sodium ion batteries, Adv. Energy Mater. 7 (2017) 1700278.
- [15] J.H. Park, T. Liu, K.C. Kim, S.W. Lee, S.S. Jang, Systematic molecular design of ketone derivatives of aromatic molecules for lithium-ion batteries: first-principles dft modeling, ChemSusChem 10 (2017) 1584–1591.
- [16] T. Liu, K.C. Kim, B. Lee, Z. Chen, S. Noda, S.S. Jang, S.W. Lee, Self-polymerized dopamine as an organic cathode for li- and na-ion batteries, Energy Environ. Sci. 10 (2017) 205–215.
- [17] S. Kim, K.C. Kim, S.W. Lee, S.S. Jang, Thermodynamic and redox properties of graphene oxides for lithium-ion battery applications: a first principles density functional theory modeling approach, Phys. Chem. Chem. Phys. 18 (2016) 20600–20606.
- [18] K.C. Kim, T. Liu, S.W. Lee, S.S. Jang, First-principles density functional theory modeling of li binding: thermodynamics and redox properties of quinone derivatives for lithium-ion batteries, J. Am. Chem. Soc. 138 (2016) 2374–2382.
- [19] T. Liu, K.C. Kim, R. Kavian, S.S. Jang, S.W. Lee, High-density lithium-ion energy storage utilizing the surface redox reactions in folded graphene films, Chem. Mater. 27 (2015) 3291–3298.
- [20] B. Häupler, A. Wild, U.S. Schubert, Carbonyls: powerful organic materials for secondary batteries, Adv. Energy Mater. 5 (2015) 1402034.
- [21] X. Han, C. Chang, L. Yuan, T. Sun, J. Sun, Aromatic carbonyl derivative polymers as high-performance li-ion storage materials, Adv. Mater. 19 (2007) 1616–1621.
- [22] X. Wu, S. Jin, Z. Zhang, L. Jiang, L. Mu, Y.-S. Hu, H. Li, X. Chen, M. Armand, L. Chen, X. Huang, Unraveling the storage mechanism in organic carbonyl electrodes for sodium-ion batteries, Sci. Adv. 1 (2015) e1500330.
- [23] G.S. Vadehra, R.P. Maloney, M.A. Garcia-Garibay, B. Dunn, Naphthalene diimide based materials with adjustable redox potentials: evaluation for organic lithium-ion batteries, Chem. Mater. 26 (2014) 7151–7157.
- [24] S. Er, C. Suh, M.P. Marshak, A. Aspuru-Guzik, Computational design of molecules for an all-quinone redox flow battery, Chem. Sci. 6 (2015) 885–893.
- [25] J.E. Bachman, L.A. Curtiss, R.S. Assary, Investigation of the redox chemistry of anthraquinone derivatives using density functional theory, J. Phys. Chem. A 118 (2014) 8852–8860.
- [26] K. Lin, Q. Chen, M.R. Gerhardt, L. Tong, S.B. Kim, L. Eisenach, A.W. Valle, D. Hardee, R.G. Gordon, M.J. Aziz, M.P. Marshak, Alkaline quinone flow battery,

- Science 349 (2015) 1529-1532.
- [27] W. Wang, W. Xu, L. Cosimbescu, D. Choi, L. Li, h Yang, Anthraquinone with tailored structure for a nonaqueous metal—organic redox flow battery, Chem. Commun. 48 (2012) 6669–6671.
- [28] T. Yokoji, H. Matsubara, M. Satoh, Rechargeable organic lithium-ion batteries using electron-deficient benzoquinones as positive-electrode materials with high discharge voltages, J. Mater. Chem. A 2 (2014) 19347–19354.
- [29] H.-G. Wang, S. Yuan, D.-L. Ma, X.-L. Huang, F.-L. Meng, X.-B. Zhang, Tailored aromatic carbonyl derivative polyimides for high-power and long-cycle sodiumorganic batteries, Adv. Energy Mater. 4 (2014) 1301651.
- [30] Jaguar version 7.6 Schrodinger, LLC, New York, NY.
- [31] S. Zhou, L.-T. Cheng, J. Dzubiella, B. Li, J.A. McCammon, Variational implicit solvation with poisson-boltzmann theory, J. Chem. Theory Comput. 10 (2014) 1454–1467
- [32] P. Winget, C.J. Cramer, D.G. Truhlar, Computation of equilibrium oxidation and reduction potentials for reversible and dissociative electron-transfer reactions in solution, Theor. Chem. Acc. 112 (2004) 217–227.
- [33] P. Winget, E.J. Weber, C.J. Cramer, D.G. Truhlar, Computational electrochemistry: aqueous one-electron oxidation potentials for substituted anilines, Phys. Chem. Chem. Phys. 2 (2000) 1231–1239.
- [34] Z. Chen, D.Y. Kim, K. Hasegawa, T. Osawa, S. Noda, Over 99.6 wt%-pure, sub-millimeter-long carbon nanotubes realized by fluidized-bed with careful control of the catalyst and carbon feeds, Carbon 80 (2014) 339–350.
- [35] D.Y. Kim, H. Sugime, K. Hasegawa, T. Osawa, S. Noda, Sub-millimeter-long carbon nanotubes repeatedly grown on and separated from ceramic beads in a single fluidized bed reactor, Carbon 49 (2011) 1972–1979.
- [36] S.P. Ong, V.L. Chevrier, G. Hautier, A. Jain, C. Moore, S. Kim, X. Ma, G. Ceder, Voltage, stability and diffusion barrier differences between sodium-ion and lithiumion intercalation materials, Energy Environ. Sci. 4 (2011) 3680–3688.
- [37] V.L. Chevrier, S.P. Ong, R. Armiento, M.K.Y. Chan, G. Ceder, Hybrid density functional calculations of redox potentials and formation energies of transition metal compounds, Phys. Rev. B 82 (2010) 075122.
- [38] Y.S. Meng, M.E. Dompablo, First principles computational materials design for energy storage materials in lithium ion batteries, Energy Environ. Sci. 2 (2009) 589–609
- [39] E.J. Son, J.H. Kim, K. Kim, C.B. Park, Quinone and its derivatives for energy harvesting and storage materials, J. Mater. Chem. A 4 (2016) 11179–11202.
- [40] X. You, M.I. Chaudhari, S.B. Rempe, S. Rick, L.R. Pratt, Dielectric properties of ethylene carbonate and propylene carbonate using molecular dynamics simulations, ECS Trans. 69 (2015) 107–111.
- [41] J.B. Goodenough, Y. Kim, Challenges for rechargeable li batteries, Chem. Mater. 22 (2010) 587–603
- [42] V. Etacheri, R. Marom, R. Elazari, G. Salitra, D. Aurbach, Challenges in the development of advanced li-ion batteries: a review, Energy Environ. Sci. 4 (2011) 3243–3262.
- [43] T. Nokami, T. Matsuo, Y. Inatomi, N. Hojo, T. Tsukagoshi, H. Yoshizawa, A. Shimizu, H. Kuramoto, K. Komae, H. Tsuyama, J.-i Yoshida, Polymer-bound pyrene-4,5,9,10-tetraone for fast-charge and -discharge lithium-ion batteries with high capacity, J. Am. Chem. Soc. 134 (2012) 19694–19700.

	Constant and any Madage also
1 2	Supplementary Materials
	Title
3	
4	Unveiled Correlations between Electron Affinity and Solvation in Redox
5	Potential of Quinone-Based Sodium-Ion Batteries
6	
7	Authors
8	Ki Chul Kim, 1,2*† Tianyuan Liu, 3† Ku Hyun Jung, 2 Seung Woo Lee, 3,4* and Seung Soon
9	Jang ^{1,4,5,6} *
10	
11	Affiliations
12	¹ Computational NanoBio Technology Laboratory, School of Materials Science and
13	Engineering, Georgia Institute of Technology, Atlanta, GA 30332, USA.
14	² Department of Chemical Engineering, Konkuk University, Seoul 05029, the Republic of
15	Korea.
16	³ G. W. Woodruff School of Mechanical Engineering, Georgia Institute of Technology,
17	Atlanta, GA 30332, USA.
18	⁴ Institute for Electronics and Nanotechnology, Georgia Institute of Technology, Atlanta,
19	GA 30332, USA.
20	⁵ Parker H. Petit Institute for Bioengineering and Bioscience, Georgia Institute of
21	Technology, Atlanta, GA 30332, USA.
22	⁶ Strategic Energy Institute, Georgia Institute of Technology, Atlanta, GA, 30332, USA.
23	Corresponding outhors.
24 25	Corresponding authors: E-mails: kich2018@konkuk.ac.kr (K. C. Kim); seung.lee@me.gatech.edu (S. W. Lee);
26	seungsoon.jang@mse.gatech.edu (S. S. Jang)
27	seungsoon.jang@mse.gateen.edu (5. 5. Jang)
28	† These authors contributed equally to this work.
29	These addicts contituded equally to this work.
30	

Energy Storage Materials Page 1 of 15

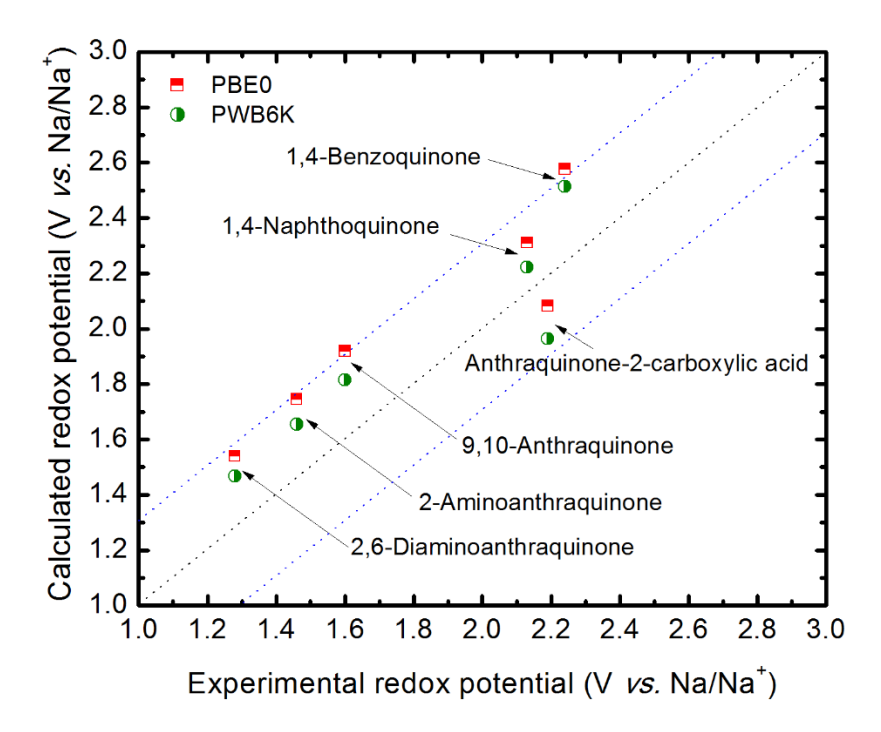
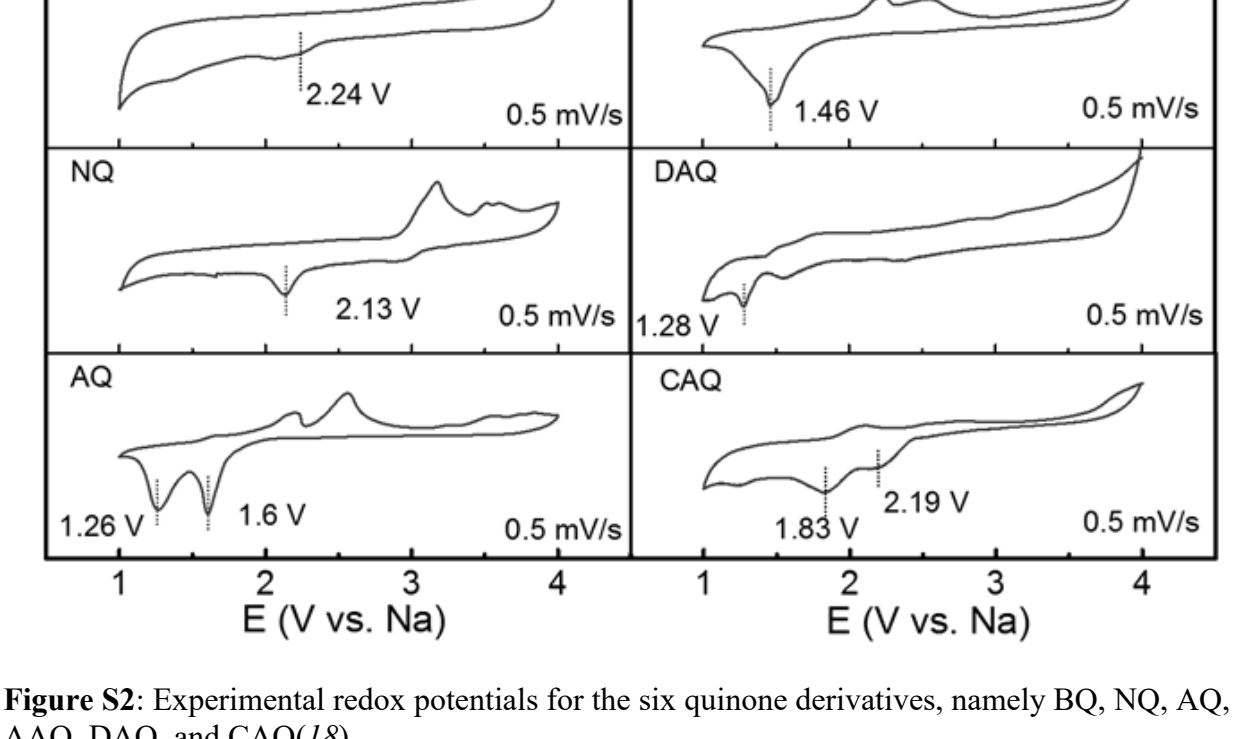


Figure S1: Experimental and calculated redox potentials of six of the quinone derivatives, namely, 1,4-benzoquinone (BQ), 1,4-naphthoquinone (NQ), 9,10-anthraquinone (AQ), 2-aminoanthraquinone (AAQ), 2,6-diaminoanthraquinone (DAQ), and anthraquinone-2-carboxylic acid (CAQ), in the absence of Li binding. Anthraquinone-2,6-dicarboxylic acid is not included because it is not available commercially. The dot lines in blue depict the the error bars to describe the deviation of the calculated redox potentials of the six quinone derivatives from their experimental values.

Energy Storage Materials Page 2 of 15



AAQ

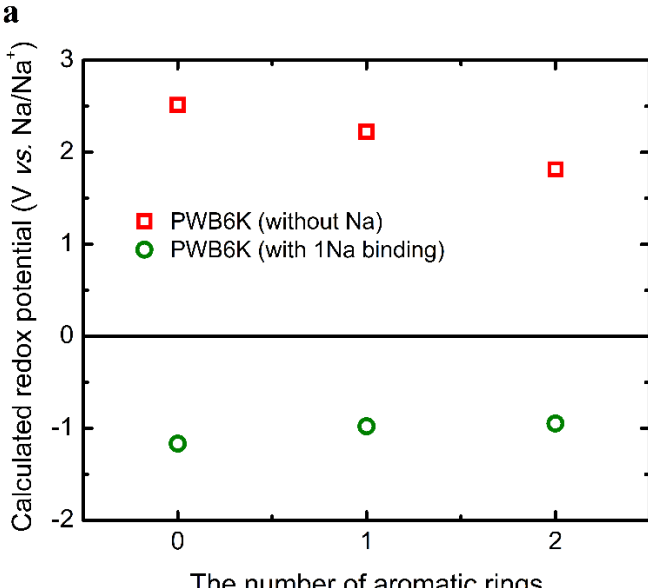
BQ

44

56 57

AAQ, DAQ, and CAQ(18).

Page 3 of 15 Energy Storage Materials



The number of aromatic rings

59

60 61

62

63

64

65

66

67

68 69

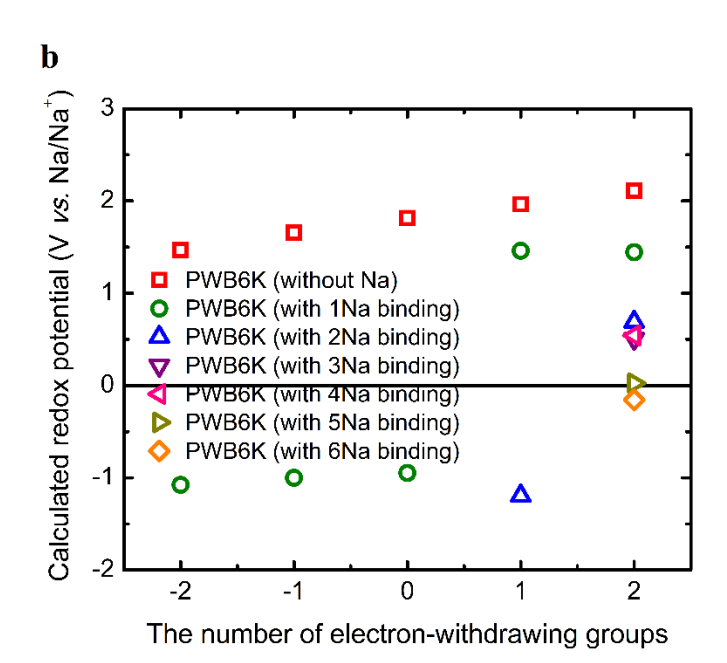


Figure S3: Correlations of the redox potential (as determined using the PWB6K functional) with (a) backbone aromaticity and (b) functionalities based on the most stable Na binding configurations. In a, the number of aromatic rings in BQ, NQ, and AQ are zero, one, and two, respectively. In b, the redox potentials are depicted as a function of the number of electrondonating (i.e., -NH₂) or electron-withdrawing (i.e., -COOH)) groups incorporated in AQ. On the x-axis, the numbers of electron-donating and electron-withdrawing groups are denoted by negative and positive integers, respectively.

Page 4 of 15 Energy Storage Materials

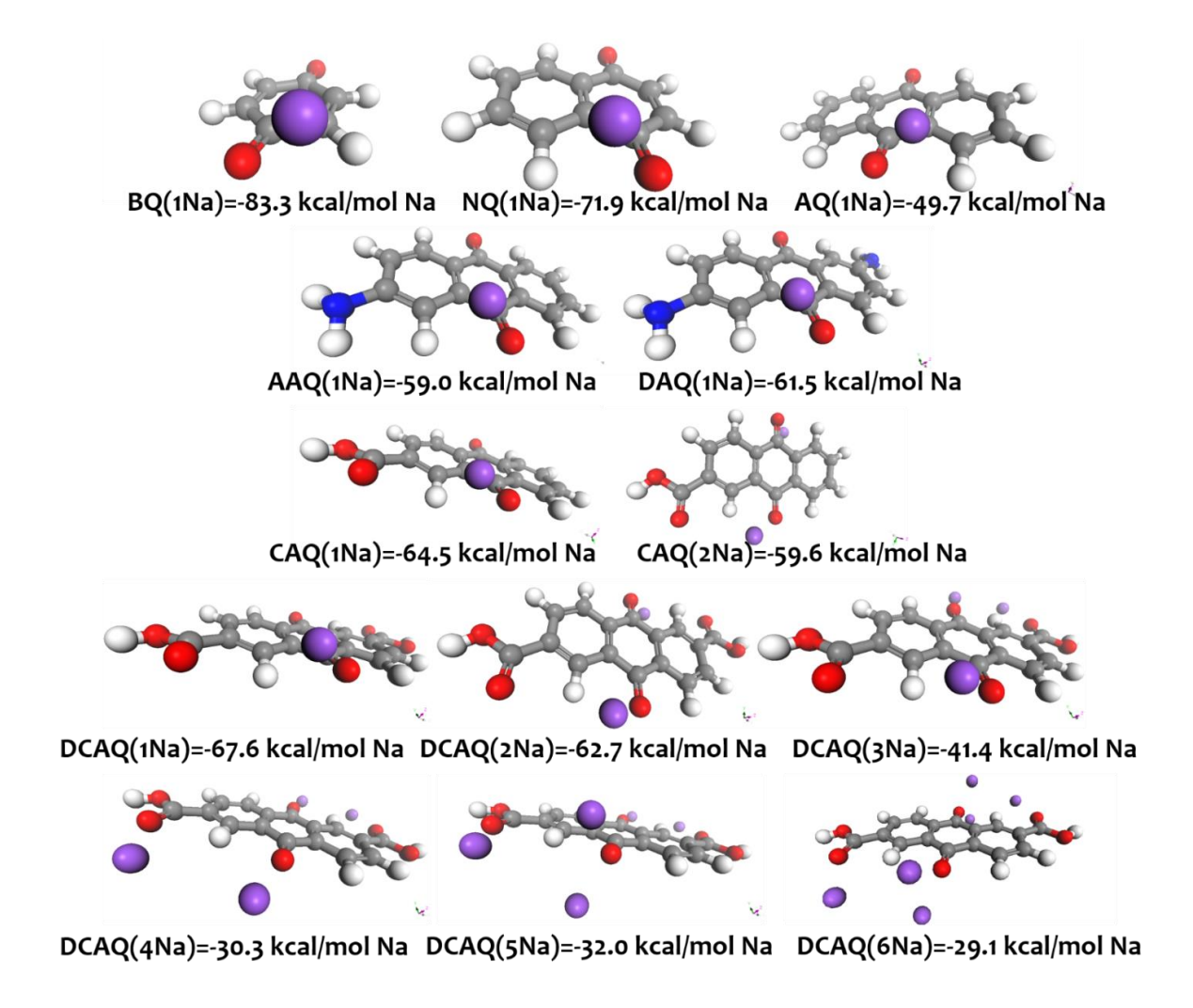


Figure S4: The most stable Na-binding configurations and average binding free energies (BFE) (in kcal/mol Na) in solution for the seven quinone derivatives, namely BQ, NQ, AQ, AAQ, DAQ, CAQ, and anthraquinone-2,6-dicarboxylic acid (DCAQ). For each quinone derivative, the most stable position of each Na atom is searched to have the lowest total energy. The atoms in gray, white, red, blue, and violet correspond to carbon, hydrogen, oxygen, nitrogen, and sodium, respectively.

Energy Storage Materials Page 5 of 15

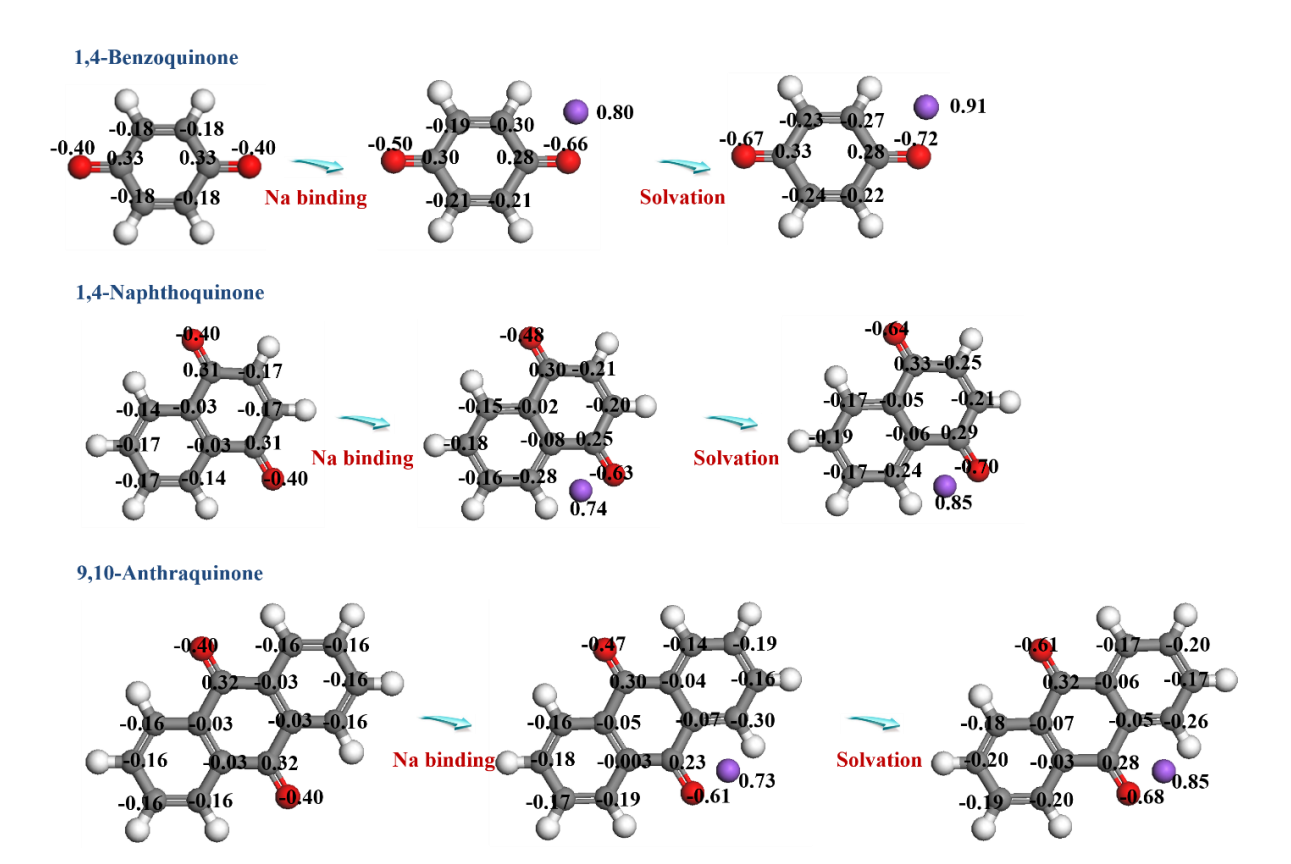
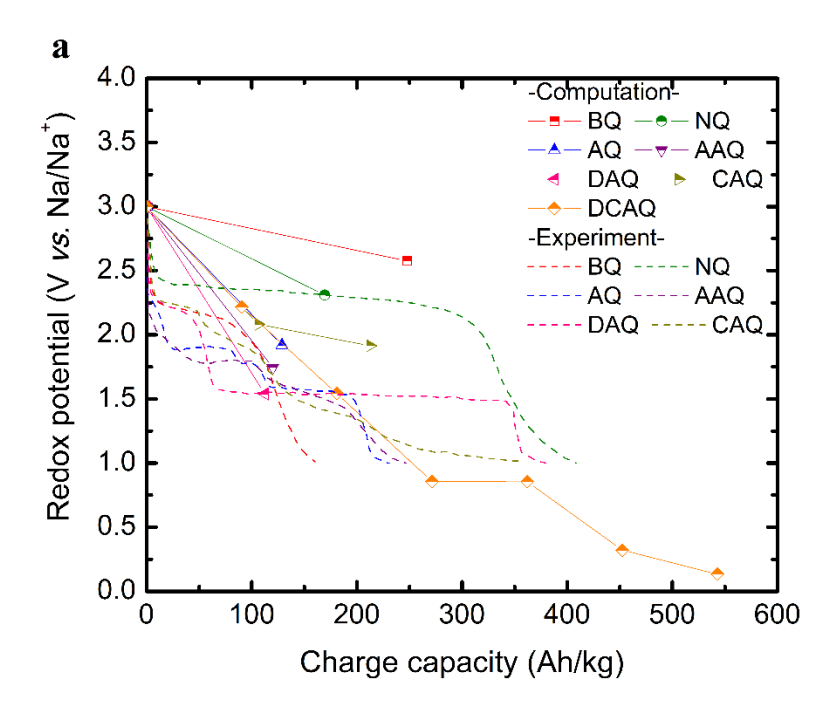


Figure S5: Atomic charges for three quinone derivatives, namely BQ, NQ, and AQ. The atoms in gray, white, red, and violet correspond to carbon, hydrogen, oxygen, and sodium, respectively.

Energy Storage Materials Page 6 of 15



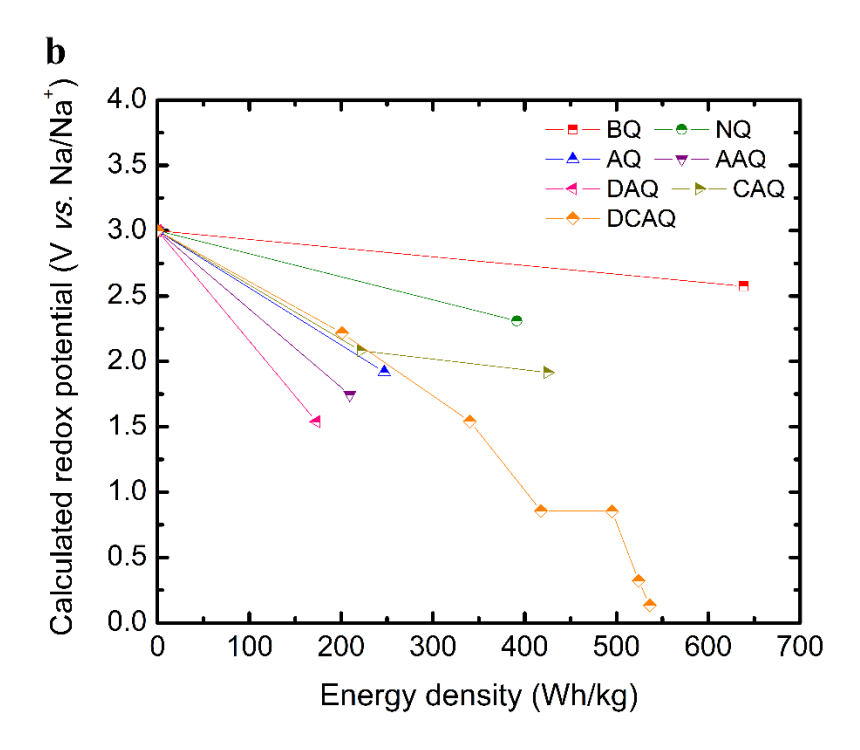
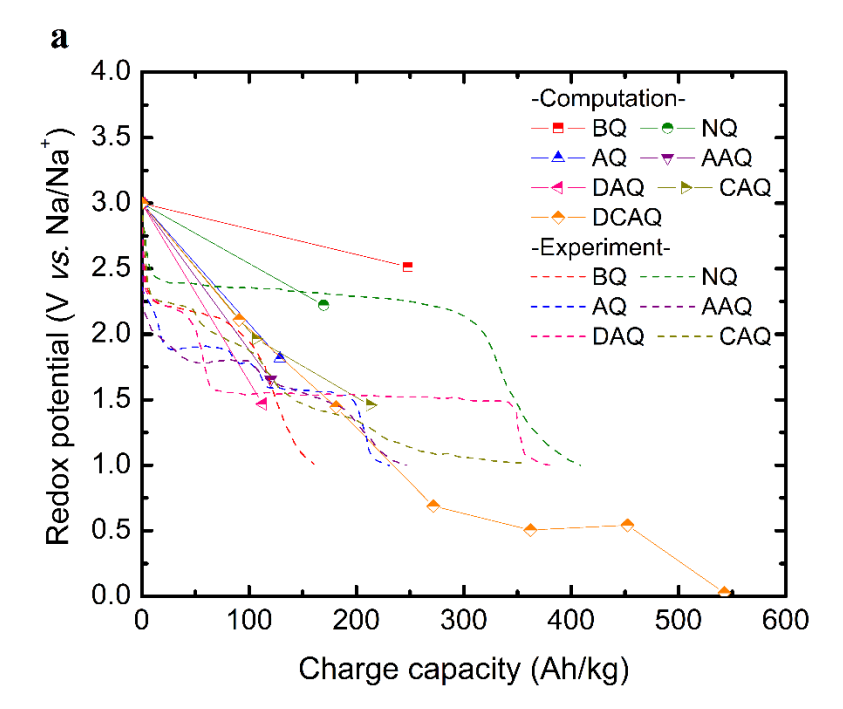


Figure S6: Profiles of the calculated redox potential (as determined using the PBE0 functional). Calculated redox potential vs. (a) charge capacity and (b) energy density for the seven quinone derivatives binding with Na atoms at the most stable positions during the discharge process. The experimentally measured charge capacities are also shown.



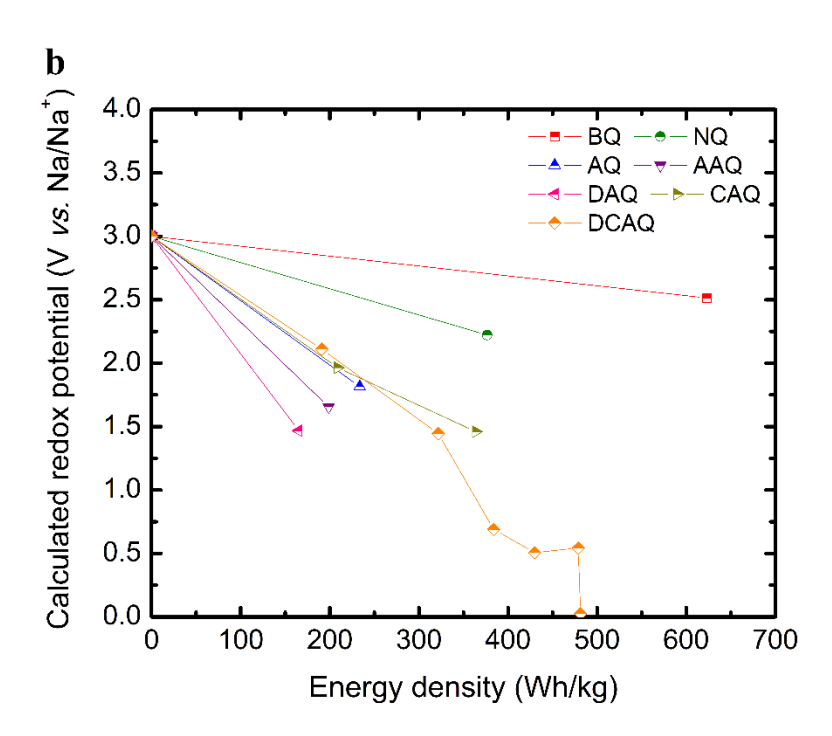
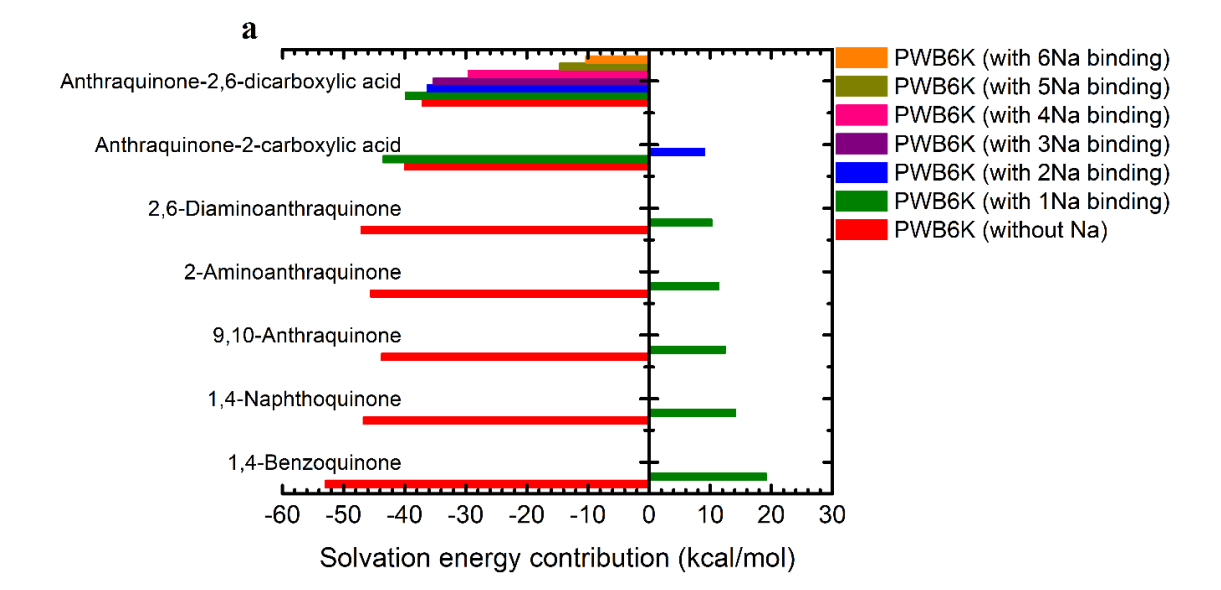


Figure S7: Profiles of the calculated redox potential (as determined using the PWB6K functional). Calculated redox potential *vs.* (a) charge capacity and (b) energy density for the seven quinone derivatives binding with Na atoms at the most stable positions during the discharge process. The experimentally measured charge capacities are also shown.

Energy Storage Materials Page 8 of 15



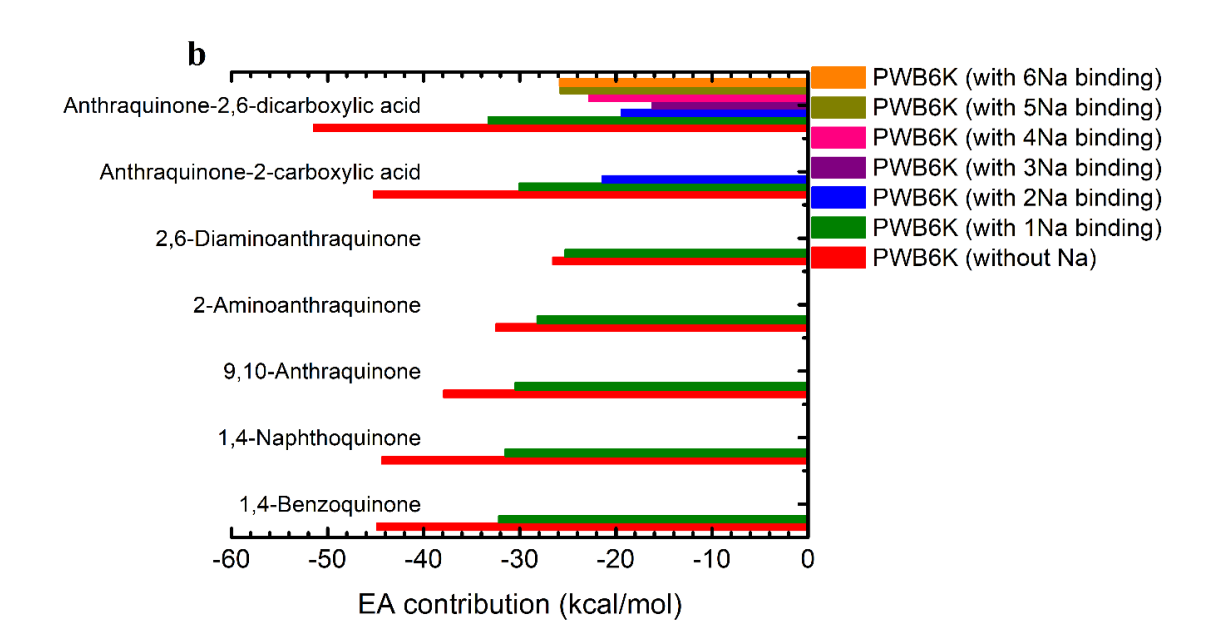


Figure S8: Contributions to the redox potentials of the seven quinone derivatives. Contributions of (a) the solvation energy and (b) electron affinity (EA) to the redox potential (as determined using the PWB6K functional) based on the most stable Na binding configuration.

Energy Storage Materials Page 9 of 15

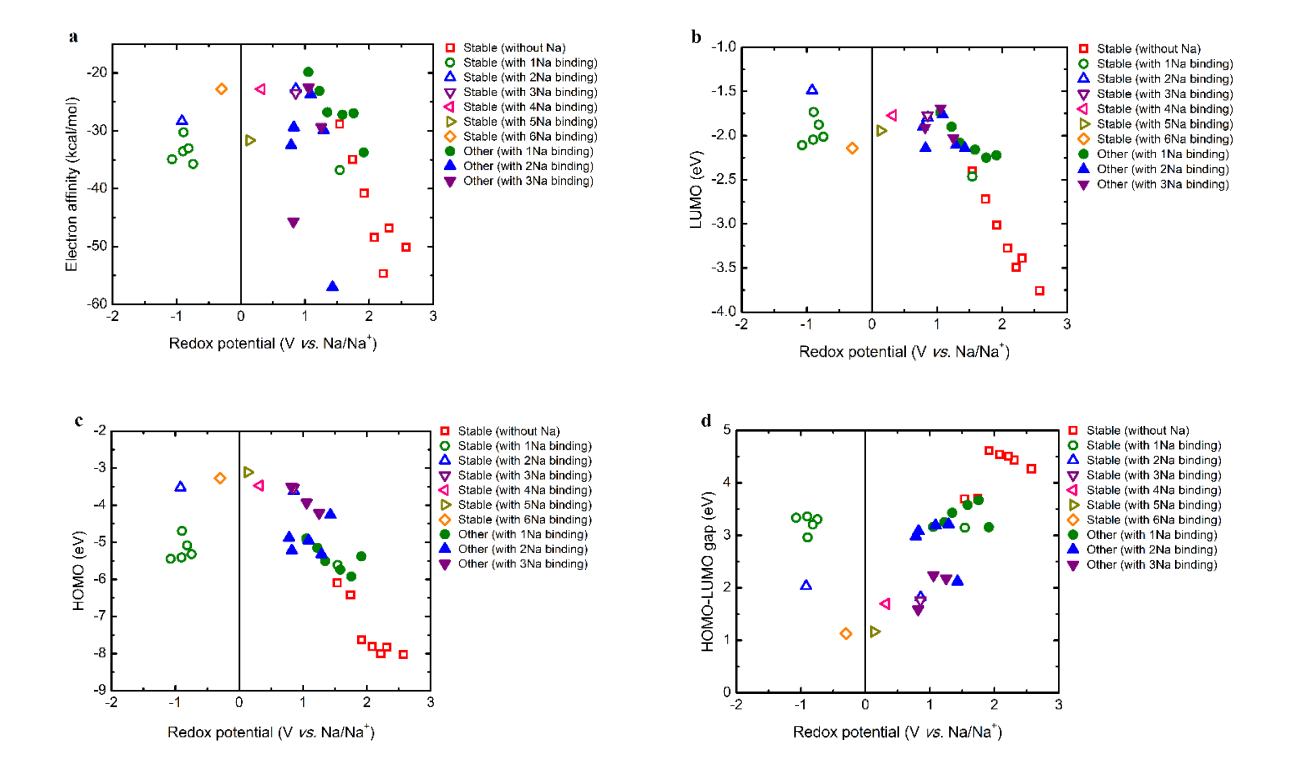
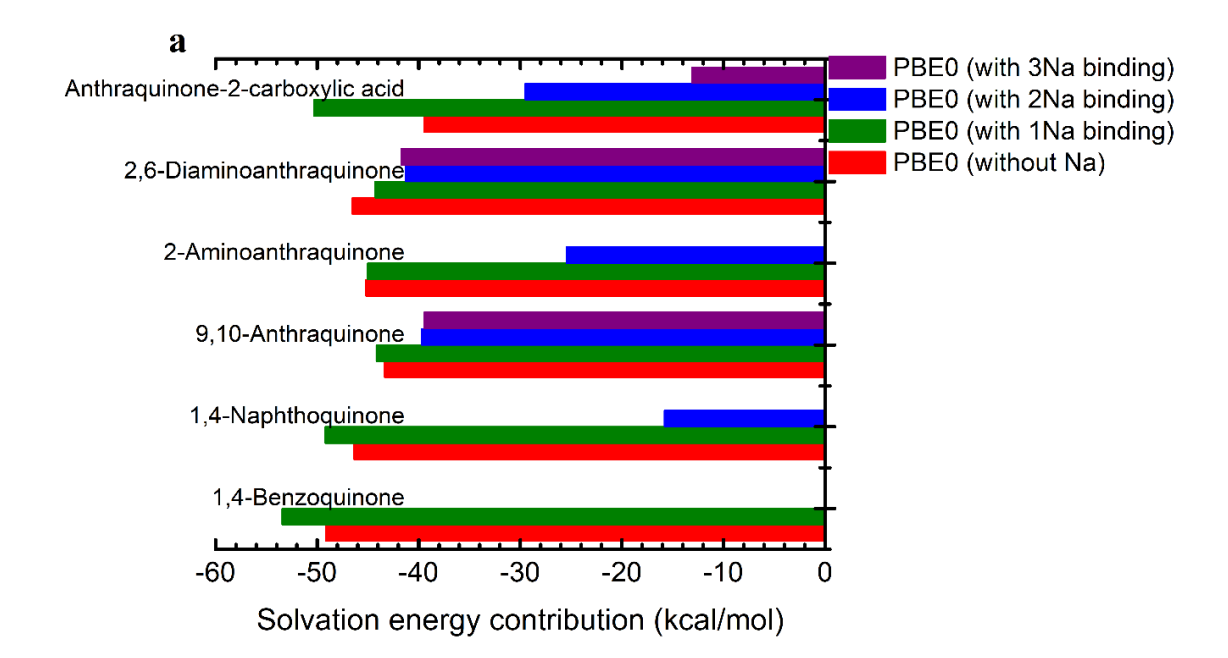


Figure S9: Correlations of the redox potential with (a) EA, (b) LUMO energy level, (c) HOMO energy level, and (d) HOMO-LUMO energy gap for the seven quinone derivatives with or without bound Na atom(s). The open and closed symbols indicate the most stable Na binding cases labeled by "Stable" and metastable Na binding cases labeled by "Other", respectively.

Energy Storage Materials Page 10 of 15



 $\begin{array}{c} 132 \\ 133 \end{array}$

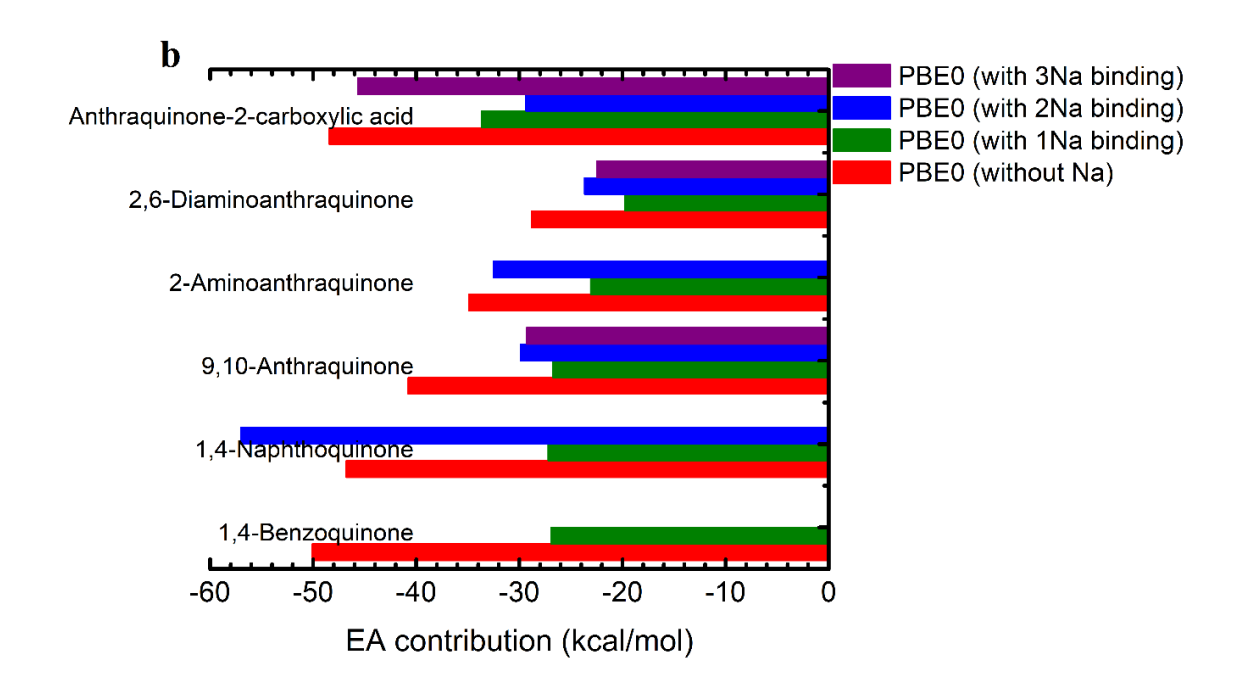
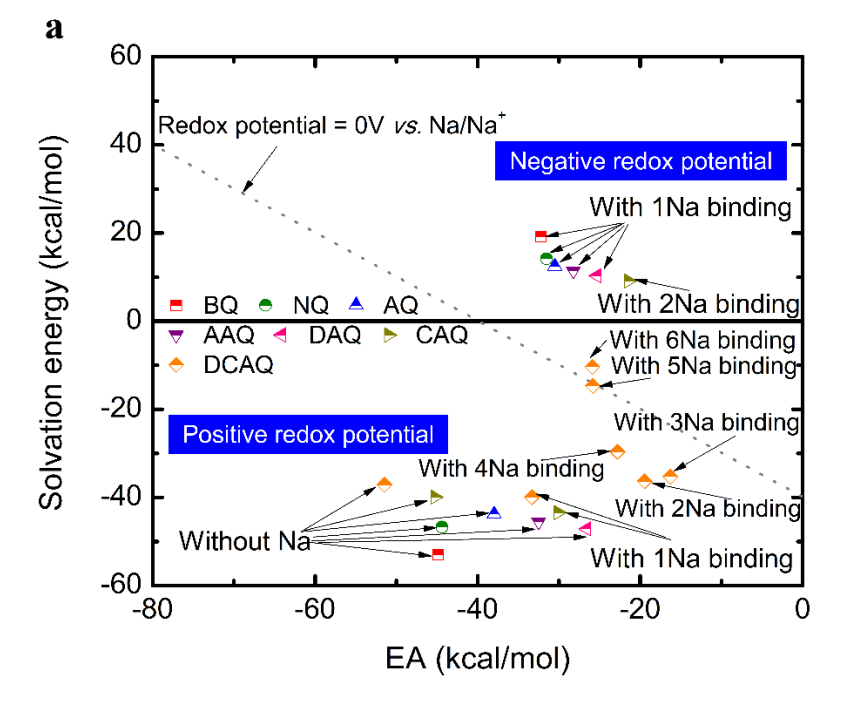


Figure S10: Contributions to the redox potentials of the six experimentally available quinone derivatives. Contributions of (a) the solvation energy and (b) EA to the redox potential (as determined using the PBE0 functional) based on the metastable Na binding configurations.

Energy Storage Materials Page 11 of 15



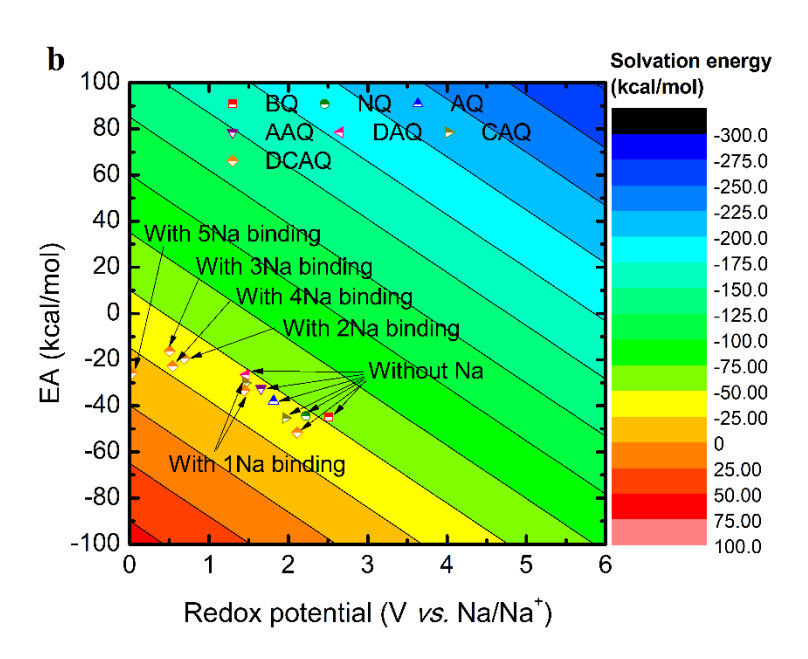


Figure S11: Correlations between the EA and the solvation energy. Correlations to (a) determine the sign of the redox potential and (b) predict a specific redox potential within the range of 0 - 6 V vs. Na/Na⁺. The data points (as determined using the PWB6K functional) correspond to the seven quinone derivatives with or without bound Na atom(s) at the most stable position(s).

Energy Storage Materials Page 12 of 15

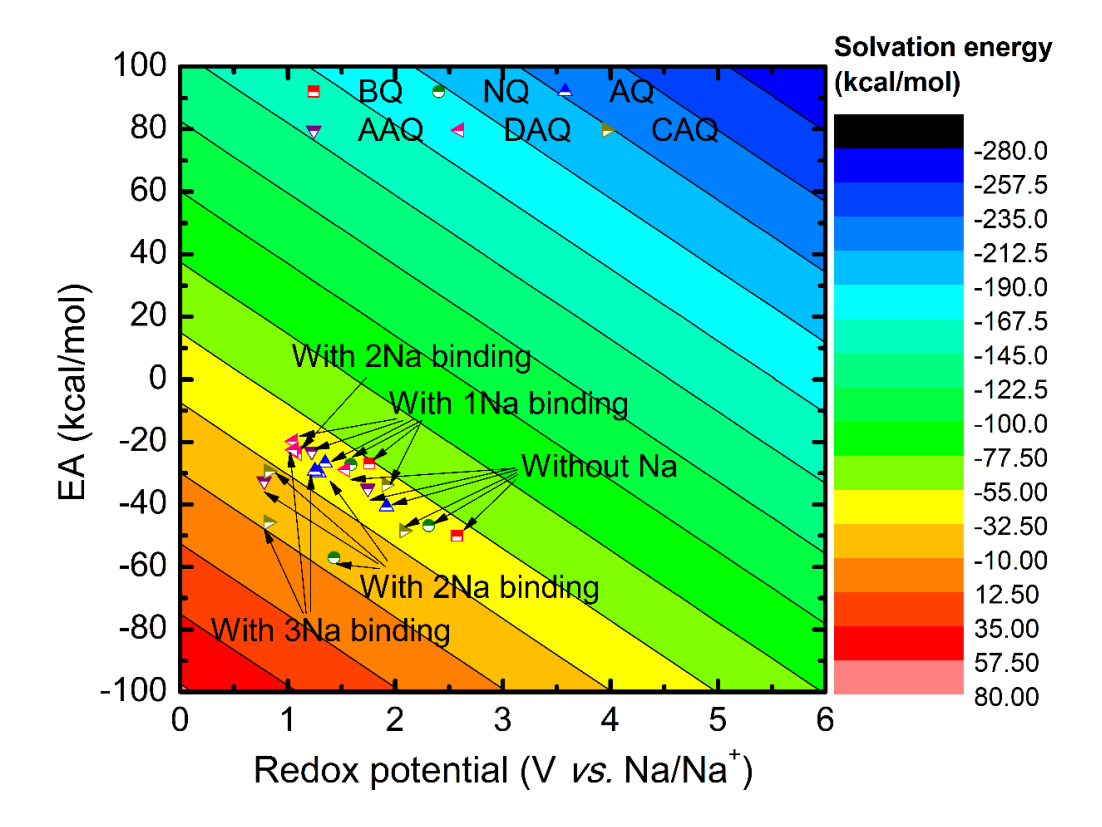


Figure S12: Correlations between the EA and the solvation energy. Correlations to predict a specific redox potential within the range of 0 - 6 V vs. Na/Na⁺. The data points (as determined using the PBE0 functional) correspond to the six experimentally available quinone derivatives with or without bound Na atom(s) at the metastable position(s).

Energy Storage Materials Page 13 of 15

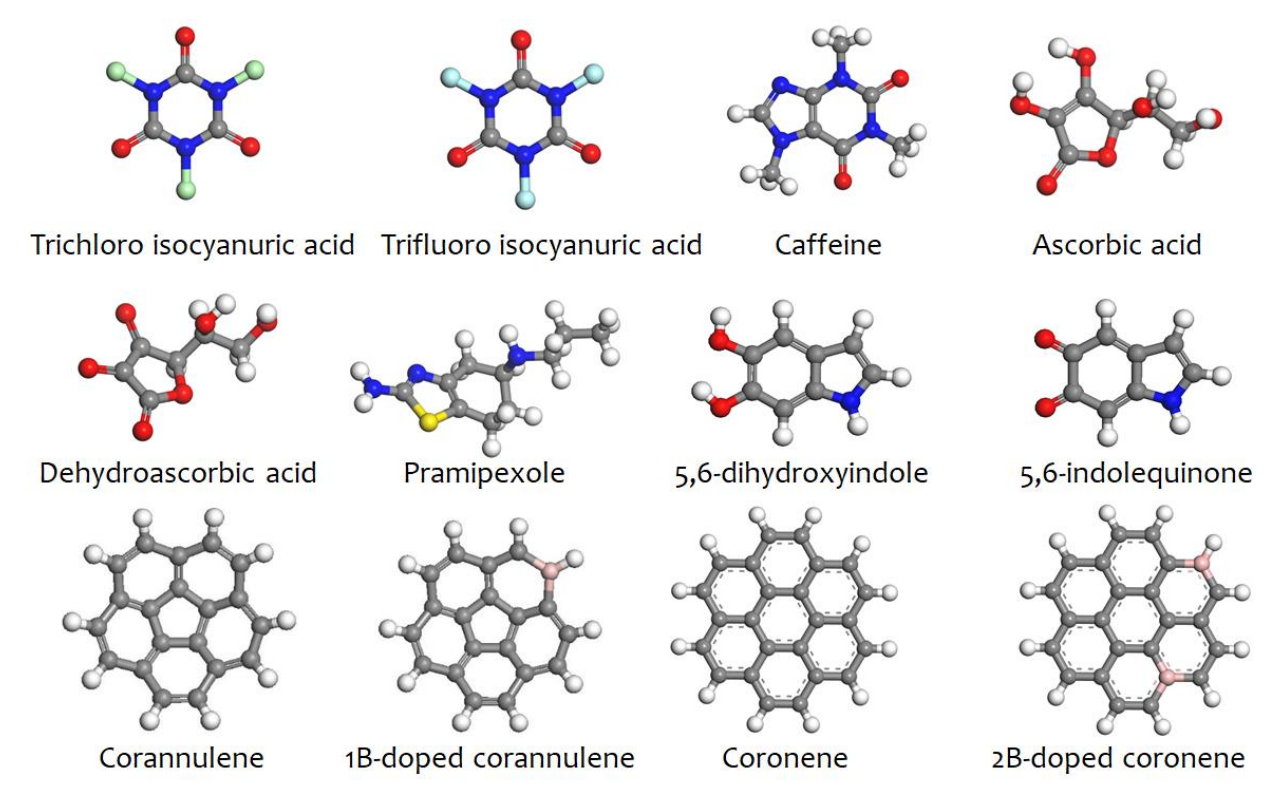


Figure S13: The structures of various organic molecules employed to verify the generalization of the suggested correlations. The atoms in gray, white, red, blue, pink, yellow, cyon, and light green correspond to carbon, hydrogen, oxygen, nitrogen, boron, sulfur, fluorine, and chlorine, respectively.

Energy Storage Materials Page 14 of 15

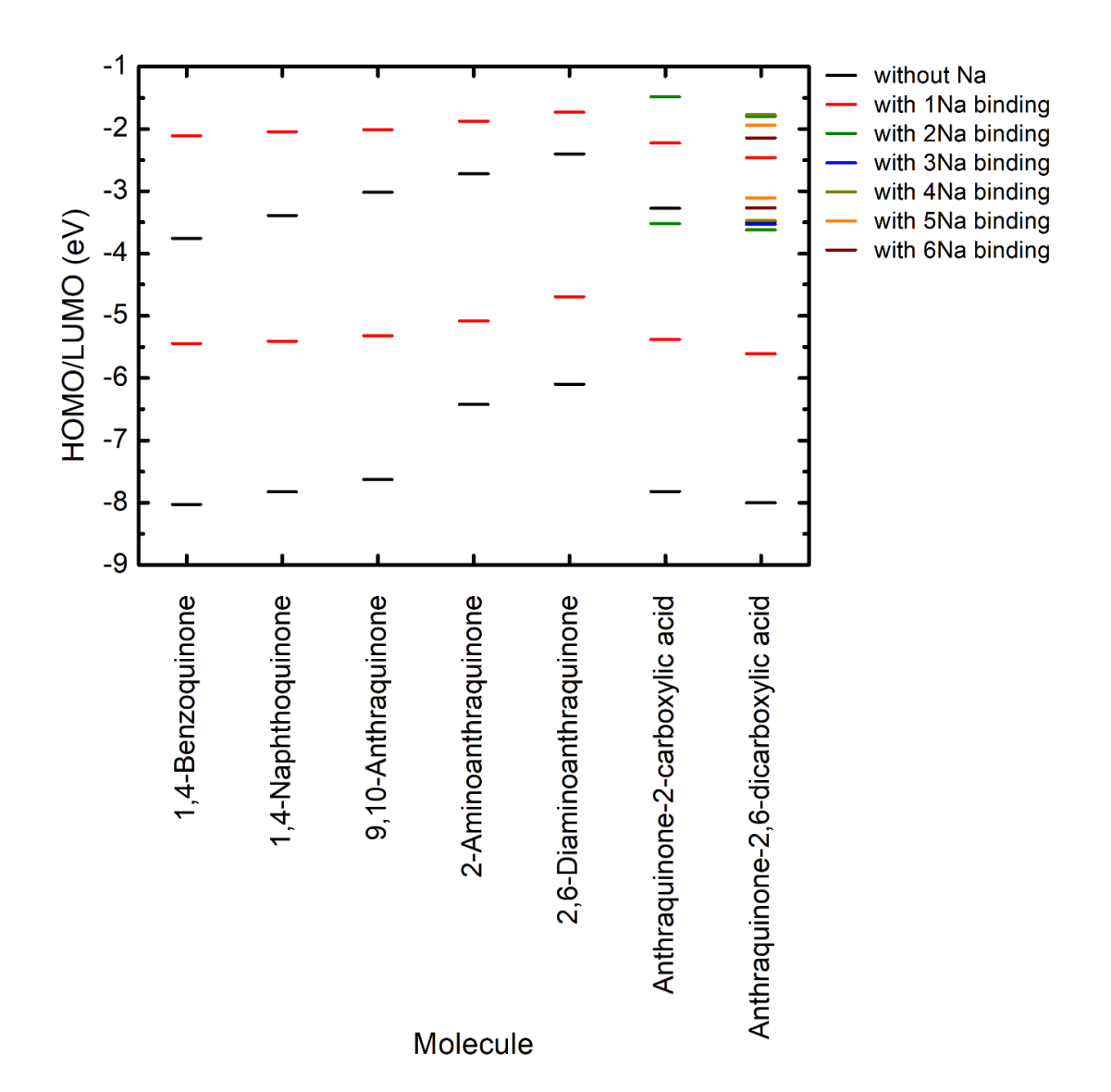


Figure S14: The energy diagrams (HOMO/LUMO) for seven quinone derivatives, namely BQ, NQ, AQ, AAQ, DAQ, CAQ, and DCAQ, with or without bound Na atom(s). In the figure, the HOMO is placed at a lower energy level than the LUMO.

Energy Storage Materials Page 15 of 15